INSTITUTE OF PHYSICS PUBLISHING PHYSICS IN MEDICINE AND BIOLOGY

Phys. Med. Biol. **47** (2002) R31–R65 PII: S0031-9155(02)07073-2

TOPICAL REVIEW

Electronic portal imaging devices: a review and historical perspective of contemporary technologies and research

Larry E Antonuk

Department of Radiation Oncology, University of Michigan, UH-B2C432, 1500 East Medical Center Drive, Ann Arbor, MI 48109-0010, USA

E-mail: antonuk@umich.edu

Received 4 July 2001
Published 1 March 2002
Online at stacks.iop.org/PMB/47/R31

Abstract

A review of electronic portal imaging devices (EPIDs) used in external beam, megavoltage radiation therapy is presented. The review consists of a brief introduction to the definition, role and clinical significance of portal imaging, along with a discussion of radiotherapy film systems and the motivations for EPIDs. This is followed by a summary of the challenges and constraints inherent to portal imaging along with a concise, historical review of the technologies that have been explored and developed. The paper then examines, in greater depth, the two first-generation technologies that have found widespread clinical use starting from the late 1980s. This is followed by a broad overview of the physics, operation, properties and advantages of active matrix, flat-panel, megavoltage imagers, presently being commercially introduced to clinical environments or expected to be introduced in the future. Finally, a survey of contemporary research efforts focused on improving portal imaging performance by addressing various weaknesses in existing commercial systems is presented.

Contents

1. Introduction R32
   1.1. Definition, role and clinical significance of portal imaging R32
   1.2. Radiotherapy film systems and the motivation for electronic portal imaging devices R33
   1.3. Prior reviews and the scope of this review R34
   1.4. Definition of measures of imager performance R35
2. Background R36
   2.1. Challenges and constraints in portal imaging R36
   2.2. A brief overview of portal imager technologies and their early development R39

3. First generation EPIDs in routine clinical use R42
3.1. Camera–mirror–lens-based EPID systems using a metal plate/phosphor screen R42
3.2. Scanning matrix ionization chamber EPID R45
4. Active matrix, flat-panel imager (AMFPI) EPIDs R46
4.1. General description of AMFPIs R47
4.2. Description of different AMFPI designs for portal imaging R48
4.3. Indirect detection active matrix flat-panel EPIDs and their advantages R49
4.4. EPIDs based on direct detection active matrix flat-panel technology R55
5. Contemporary research toward improving EPID performance R55
6. Conclusion R60
Acknowledgments R61
References R61

1. Introduction

1.1. Definition, role and clinical significance of portal imaging

Over the last half century, the treatment of cancer by means of external beams of megavoltage x-ray radiation has benefited from a variety of significant technical advances. These advances include: the development of relatively compact, gantry-mounted linear accelerators capable of isocentric delivery of high-dose x-rays; the adoption of novel three-dimensional imaging modalities (CT, MRI, PET, SPECT and ultrasound) capable of providing a wealth of anatomical and functional information useful for planning radiotherapy treatments; the creation of treatment planning software systems which provide a means of exploiting 3D imaging information; and the development of hardware (such as laser alignment systems, adjustable treatment tables and multi-leaf collimators) and software (such as record-and-verify systems) which facilitate the delivery of ever more sophisticated treatment plans. Furthermore, recent years have witnessed efforts to employ novel combinations of these tools, such as treatment machines integrated with CT scanners and digitally controlled multi-leaf collimators used to carry out complex treatment plans via intensity-modulated radiotherapy techniques. Generally, these advances have helped to further a central aim of radiotherapy—maximizing the dose delivered to the tumour while minimizing the dose to surrounding healthy tissues. Towards accomplishing this objective, the tumour region is commonly irradiated from a number of directions with suitable radiation fields or *ports*.

Despite these and many other advances, verifying that each *radiation port* is being delivered as intended remains a difficult practical issue due to a number of complicating factors. For example, the size and shape of the tumour can change during the course of treatment, which typically extends over a number of weeks. In addition, the position of the tumour in the patient may vary from treatment to treatment, or even during treatment, due to such influences as breathing, the degree of extension of the bladder and changes in patient positioning. Moreover, errors in the set-up of the patient and/or of the beam collimators are also possible. For these reasons, it has long been recognized that the use of the therapy x-ray beam itself to create *portal images* can be of significant benefit in assuring correct delivery of the radiation dose. (The use of diagnostic x-ray imaging in the treatment room is also a potentially powerful method to assist in patient positioning and the object of considerable, complementary research. However, this topic is beyond the scope of the present review.) *Localization imaging* refers to the creation of portal images using a small fraction of the treatment dose prior to the delivery of the main dose while *verification imaging* refers to the creation of portal images during the actual treatment. In the case of localization imaging,

Figure 1. Picture of a radiotherapy film cassette. Such devices typically have dimensions of approximately 35 cm × 43 cm × 1.4 cm.

the objective is to view the image before proceeding with the main treatment so as to allow for the possibility of adjustment of the treatment set-up. Verification imaging, on the other hand, serves to provide a record of how the treatment was performed—although, in principle, adjustment of the patient set-up during treatment is also possible provided that the image(s) can be viewed and/or processed in real-time.

1.2. Radiotherapy film systems and the motivation for electronic portal imaging devices

Historically, portal imaging has been performed primarily through the use of radiotherapy film cassettes (figure 1). In conventional portal film systems, a sheet of film is sandwiched between a front metal plate (typically an ∼1 mm copper plate) and a rear plastic or metal plate. By detecting the incident x-rays, the front plate acts as a build-up layer that generates high-energy electrons which expose the film. In addition, this front layer serves to block scattered secondary radiation incident on the cassette—radiation which would otherwise result in a loss of contrast. The back plate serves as an electron backscatter material. Along with the overall design of the cassette, the back plate also helps to ensure good contact between the film and the surrounding materials thereby contributing towards the preservation of image quality.

Portal films can be divided into two categories, distinguished by their sensitivity: *localization films* provide images using a small amount of radiation (typically ∼4 to 6 monitor unit (MU) irradiations) while *verification films* provide images using the entire treatment dose (typically ∼30 to 80 MUs). (A monitor unit corresponds to the delivery of $\sim 1 \times 10^{-2}$ Gy in tissue or a tissue-equivalent phantom under conditions defined by the personnel responsible for the dosimetry of a given machine—for example, in the centre of a 10 cm × 10 cm field, at the isocentric distance of the treatment machine, at a depth of 10 cm below the phantom surface.) The image quality provided by film cassettes, although constrained by the nature of the radiotherapy application, as explained in the following section, is sufficient to provide significant, useful information for the tasks of localization and verification. The quality of images provided by film cassettes using conventional film has effectively served as a gold standard against which the quality of new systems is commonly compared.

A recent innovation has further improved the quality of portal images produced with film (Dickerson *et al* 1997). Enhanced contrast localization (EC-L) systems use a fine-grained, very low speed, high gamma graphics art film sandwiched between two phosphor screens along with a front ∼1 mm copper plate. As outlined in Munro (1999), this system offers a variety of advantages over systems using conventional film. The presence of the phosphor screens improves the efficiency of detection of the incident x-ray quanta by a factor of 2 thereby improving the overall image quality. The system virtually eliminates film noise (through the use of a very fine grain structure in the film) leading to a noticeable improvement in the visual quality of the resulting images. Finally, the EC-L film has a considerably larger gamma (and thus a higher display contrast) than that of conventional films (by a factor of ∼3.5) which improves the display of the low contrast objects typically found in megavoltage images.

Despite the fact that radiotherapy film cassettes represent a compact, lightweight technology and provide useful image information, they suffer from several major disadvantages. Since the film must be removed from the cassette and developed in a film processor, there is a gap of several minutes between exposing the film and obtaining information from it. In the case of localization imaging, this introduces a significant delay during which the information content of the film may become invalid (e.g. due to patient movement). In addition, as this delay adds significantly to the overall treatment time for a given patient, it discourages frequent localization checks so that many institutions perform such checks, at most, once a week. In the case of verification imaging, the use of film cassettes does not provide the possibility of monitoring the accuracy of treatment during the course of the delivery of a given portal field. As in diagnostic radiography, film cassette technology suffers from the additional limitation that the film generally serves as both the capture and display medium—imposing restrictions upon its design so as not to seriously compromise either function and requiring transport of the film from the treatment room to a developer and then to a viewing box. Although it is certainly possible to render the film image into digital form using a film digitizer, this seldom happens in a practical clinical setting. Consequently, digital manipulation and processing of the image so as to accentuate some aspect of the information is precluded as is the possibility of electronic archiving. Finally, film systems offer a relatively limited range of exposures (i.e. a narrow latitude) over which the image is neither under- nor over-exposed. This limitation is even more accentuated with the EC-L systems since the increased gamma comes at the expense of an even narrower latitude. These weaknesses in radiotherapy film technology have served as a powerful incentive for the development of electronic portal imaging devices offering real-time, digital readout.

1.3. Prior reviews and the scope of this review

A number of previous papers have provided excellent reviews of the history and development of portal imaging technologies. Boyer *et al* (1992) contains a general review of the physics of megavoltage imaging along with a detailed description of the operational principles of most of the electronic portal imaging devices that had been developed to that point. Roehrig and Cheng (1993) summarize portal-imaging-related issues concerning x-ray detection, contrast, signal-to-noise ratio, detective quantum efficiency (DQE, discussed below) and spatial resolution before providing a brief description of many of the approaches applied to electronic portal imaging. Webb (1993) provides an insightful description and analysis of a wide variety of electronic and non-electronic portal imaging technologies as well as related imaging matters. Shalev (1995) touches briefly on portal imaging technologies and comparisons of some of these technologies.

Munro (1995) briefly reviews the history of portal imaging before concentrating primarily on the two EPID technologies that were commercially available at the time as well as those which showed particular future promise. That paper concludes with a detailed description of various image registration techniques used to identify geometric errors from portal images. Also, Munro (1999) presents a highly detailed review of the history and technology of electronic and non-electronic portal imagers along with a discussion of a variety of theoretical and practical considerations and issues. That study also summarizes, in tabular form, features of the two EPID technologies commercially available at the time. Finally, Herman *et al* (2001) presents comprehensive information about the physics, technology and features of the same two commercially available EPID technologies covered by prior reviews as well as detailed information on procedures for successful clinical implementation, software tools, clinical protocols and quality assurance requirements.

The present paper presents a brief overview of the challenges and constraints on electronic portal imaging devices imposed by the nature of the application and the physics of the imaging source. This is followed by a concise historical review and perspective on the various classes of technologies that have been developed to meet these requirements. A more detailed operational description is then provided for the two first-generation portal imaging technologies that were commercialized and widely implemented starting from the late 1980s. Next, a detailed description of a new, high performance, portal imaging technology, which is presently undergoing commercial introduction and which emerged from research initiated in the late 1980s, is presented. Finally, a review of recent research, motivated by limitations in existing commercial systems, is given.

1.4. Definition of measures of imager performance

A brief introduction to the meaning and importance of a number of metrics that quantify, in an objective, observer-independent manner, the performance of x-ray imaging systems follows. In an imaging system, the number of incident x-ray quanta and the variation in this number represent the signal and noise input to the system. In general, it is desirable to design a system that, for a given input, produces as high a signal-to-noise ratio (SNR) at its output as possible, since this is requisite to good image quality. The function of an imaging system is to transform the information content of the input quanta into an observable output. In an ideal system, the input SNR ($\mathrm{SNR_{in}}$) passes through the system without degradation (i.e. $\mathrm{SNR_{out}} = \mathrm{SNR_{in}}$). DQE is a widely accepted measure of the performance of x-ray imaging systems and is often defined as follows (Shaw and Dainty 1976, Metz *et al* 1995, Cunningham and Shaw 1999):

$$\mathrm{DQE} = \frac{\mathrm{SNR_{out}^2}}{\mathrm{SNR_{in}^2}} \qquad (0 \leqslant \mathrm{DQE} \leqslant 1). \tag{1}$$

It is very desirable that the DQE of a system be large and as close to 1 as possible. (DQE is also frequently expressed as a per cent with 100% representing the theoretical maximum.) Knowledge of the DQE is therefore essential for a complete characterization of system performance and such characterization is commonly performed for x-ray imaging systems. More generally, the detective quantum efficiency can be determined as a function of spatial frequency, f—an appropriate independent variable for an x-ray imaging system. The frequency-dependent detective quantum efficiency, $\mathrm{DQE}(f)$, may be expressed (Dobbins *et al* 1995, Cunningham and Shaw 1999) in terms of the following measurable (or calculable) quantities: (i) the mean incident x-ray fluence, $\bar{q}$; (ii) two other spatial-frequency-dependent measures of system performance: modulation transfer function, $\mathrm{MTF}(f)$

Figure 2. View of a typical radiotherapy treatment machine along with its treatment table.

(a measure of the spatial resolution of a system) and noise power spectrum, NPS(f) (a measure of the noise properties of a system) and (iii) the mean detector signal, $\bar{d}$, which can be derived from data used in the determination of the NPS(f):

$$\mathrm{DQE}(f) = \frac{\bar{d}^{\,2}\mathrm{MTF}^2(f)}{\bar{q}\mathrm{NPS}(f)} \qquad (0 \leqslant \mathrm{DQE}(f) \leqslant 1). \tag{2}$$

An insightful description of the meaning and relationship of the quantities appearing in equation (2) appears in Cunningham and Shaw (1999). It is of interest to point out, for a given imager design, an upper limit on the magnitude of the DQE is given by the fraction of the incident x-rays that generate useful signal in the x-ray converter—although other factors such as MTF(f), Swank noise and non-x-ray-quantum-related noise can further limit the DQE (Cunningham and Shaw 1999).

2. Background

2.1. Challenges and constraints in portal imaging

The considerable cost of a shielded treatment room and the equipment within strongly encourages efficient use of these facilities. A premium is therefore placed on performing patient treatments expeditiously (typically in ∼10 to 20 min per patient) so as to maximize their use. Figure 2 shows a typical linear accelerator and treatment table. For such equipment, the treatment gantry rotates ±180° along a 1 m radius around the mechanical isocentre of the machine while the treatment table typically offers several degrees of horizontal, vertical and rotational adjustments. In this environment, it is important that the presence of the portal imaging device does not significantly interfere with the degrees of freedom offered by the gantry and table. Nor should the portal imager hinder the ability of the radiation therapists

to quickly position the patient on the treatment table prior to treatment delivery. While these requirements are relatively well satisfied by a radiotherapy film cassette (due to its compact size and portability), an electronic portal imager is generally more cumbersome and far less portable. For this reason, and to help guarantee that the imager will always be appropriately positioned during imaging, EPIDs are typically attached onto the gantry on the opposite side of the isocentre relative to the radiation source. In order to minimize the degree to which the imager restricts treatment positions or encumbers the therapist, it is highly desirable that an EPID be compact and capable of being easily removed (or retracted towards the gantry) when not in use.

Further challenges on portal imager design arise due to the fact that portal imaging must take place in an environment and with a radiation source which are optimized for treating the tumour, and not for producing the highest quality images. (This differs from the situation in diagnostic radiology where, since the primary goal is to produce excellent image quality, the design of the radiation source, detector and environment are optimized to provide the highest quality image.) Generally, the image quality in portal imaging is strongly constrained by the low contrast and limited spatial resolution possible given the nature of the high-energy radiation sources used for therapy. An important factor limiting contrast in portal images is the fact that x-ray attenuation is dominated by Compton interactions at therapy energies, as opposed to photoelectric interactions at diagnostic energies. The probability of Compton interactions is highly dependent on the electron density of the material, unlike photoelectric interactions, which show a strong dependence on atomic number. Since anatomical structures generally provide relatively small variations in electron density, the image contrast at therapy energies is inherently more limited than at diagnostic energies (Herman *et al* 2001). Similarly, a factor limiting spatial resolution in portal images is the large focal spot size of therapy machines, approximately one to several millimetres (Munro *et al* 1998)—over an order of magnitude larger than that commonly associated with diagnostic x-ray sources. Such large focal spot sizes contribute to a loss in spatial resolution in therapy imaging comparable, for example, to the loss due to photon and electron scatter within the x-ray converter in radiotherapy film cassettes (Munro *et al* 1998). For this reason, most electronic portal imager designs incorporate elemental detection elements (e.g. pixels) with dimensions in the range of ∼0.5–2 mm—compared to a range of ∼0.05–0.5 mm for the majority of technologies serving diagnostic x-ray imaging applications.

Another constraint relates to the fact that the x-ray photons that make up the radiotherapy beams used for portal imaging have a significantly lower probability of interaction with matter than for the lower energy x-rays used in diagnostic imaging. As a consequence, the fraction of the radiotherapy beam that generates detectable signal in the converter (called the x-ray quantum detection efficiency) is typically low. For example, it is only ∼1% for conventional portal film used with a metal plate (Herman *et al* 2001). For converters commonly incorporated in commercially available EPIDs (discussed in later sections) which consist of some form of metal plate in contact with either a liquid ionization medium or with a phosphor screen, the absolute proportion of the incident beam detected is only slightly larger: ∼1.5 times and ∼2 to ∼4 times higher, respectively (Herman *et al* 2001). These relatively low detection efficiencies impose a correspondingly low upper limit on the DQE performance of EPIDs employing such converters. (The DQE of a standard radiotherapy localization cassette and of other combinations of film and metal plates has been examined with radiotherapy beams and found to be significantly below 1%—limited by noise associated with film granularity (Munro *et al* 1987).) By comparison, the maximum DQE values for diagnostic x-ray imaging systems commonly range from 20 to 80%. Fortunately, even with such low detection efficiencies, radiotherapy beams contain such large fluences of x-rays

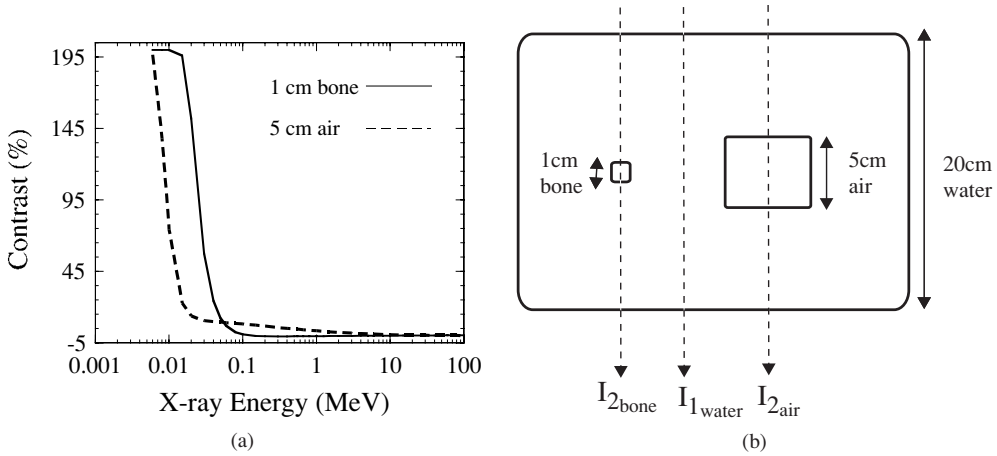

Figure 3. (a) Graph illustrating calculations of contrast as a function of monoenergetic x-ray energy. Results are shown for 1 cm of bone and 5 cm of air, both immersed in a 20 cm water phantom and calculated using equation (1). (b) Drawing corresponding to the geometry of the two sets of calculations shown in (a).

per unit dose (Rogers 1984) that considerable spatial and contrast image information can nevertheless be obtained from radiotherapy cassettes and commercial EPID designs using only a few monitor units of radiation.

The information content of portal images is further limited by the small differences in attenuation between various anatomical features at therapy energies resulting in limited contrast. A common measure of the contrast provided by an object (which, however, ignores the effect of scatter (Herman *et al* 2001)) is given by the expression (Antonuk *et al* 1994)

$$C(\%) = 200\frac{(I_2 - I_1)}{(I_1 + I_2)} \tag{3}$$

where I_1 is the radiation transmitted through the phantom in the absence of the object to be observed and I_2 is that transmitted through the phantom in the presence of the object. Figure 3(a) contains a graph of contrast, as calculated using equation (1), as a function of monoenergetic x-ray energy. The calculations shown correspond to two situations depicted in figure 3(b): a 1-cm thick segment of bone and a 5-cm thick pocket of air, each immersed in 20 cm of water—situations which are radiologically representative of normal human anatomy. The large values of contrast at lower x-ray energies exhibited in figure 3(a) are indicative of the ability of diagnostic-quality x-rays (∼20–150 kVp) to provide a large amount of information. Conversely, the contrast at higher energies is considerably smaller and, consequently, portal images (acquired with ∼1–50 MV beams) exhibit considerably less information. Therefore, portal imagers should be designed to provide a high degree of contrast sensitivity in order to provide reasonable image quality.

In addition to providing real-time image readout and presentation, the design of a portal imaging device faces a number of additional challenges. For example, the imager must be capable of withstanding the large cumulative doses associated with the application—potentially as high as 1×10^4 to 2×10^4 Gy per year if used frequently (Boudry and Antonuk 1996). It is also desirable that the design of a given imager be capable of operating over a large range of doses—ideally providing high quality images from the lowest doses deliverable by the treatment machine (typically 1 MU) up to the entire treatment dose. The

nature of a given imaging technology usually defines a narrow range of dose to the detector over which the device is capable of generating clinically useful, individual images. For modern EPIDs, this range usually lies somewhere between 1 and 10 MUs. (Of course, with a digital imaging device, it is often possible, if the hardware allows it, to capture and sum consecutive images so as to provide a frame-averaged result—thereby extending the range of operation.) Moreover, it is highly desirable that the quality of the image be limited by the statistical noise of the x-ray quanta that are detected, rather than by some other competing noise source (such as noise from the acquisition system electronics). The achievement of such a condition, called *x-ray quantum-limited imaging* (or, alternatively, *input quantum-limited imaging*), implies that for the number of x-ray quanta detected, the image quality cannot be improved. Generally, this condition is most challenging to accomplish at low doses since the number of detected x-rays (and hence x-ray noise) is minimal.

2.2. A brief overview of portal imager technologies and their early development

A considerable amount of ingenuity and innovation has been applied to the design of electronic portal imaging systems since the late 1950s. A summary of the wide variety of technologies that have been explored appears in table 1. The organization of this table represents a division of technologies into those which involve the generation of light (optical systems) and those which do not (non-optical systems). A further delineation is made between technologies that are sensitive to the entire portal radiation field simultaneously (two-dimensional, area detectors) and linear arrays of detectors that are scanned across the radiation field (one-dimensional detectors). For a given x-ray converter, a configuration providing simultaneous detection over a two-dimensional area will make more efficient use of the incident radiation thereby generally allowing higher quality images at equivalent or lower doses than for a linear scanning system.

The published literature suggests that the development and use of electronic portal imagers began in the 1950s. One pioneering system, used to monitor treatment with 200 kV x-rays in real-time, consisted of an x-ray image intensifier tube whose light output was optically coupled via a mirror–lens arrangement to a Vidicon TV camera (Strandqvist and Rosengren 1958, Wallman and Stalberg 1958). Another early system, used to monitor treatment with x-rays generated by a 2 MeV Van der Graff accelerator, comprised a fluorescent screen which was coupled to an Orthicon camera via a mirror–lens combination (Andrews *et al* 1958)—an approach later modified through the important addition of a metal plate in front of the fluorescent screen (Benner *et al* 1962). Interest in the general approach of optically coupling a metal plate/phosphor screen to a camera via a mirror–lens combination, schematically illustrated in figure 4, greatly increased following the introduction of relatively modern hardware to the technique by Baily *et al* 1980. This approach was further developed and refined through the technical, theoretical and clinical efforts of a number of groups (Leong 1986, Shalev *et al* 1989, Munro *et al* 1987, 1988, 1990a, 1990b, Ezz *et al* 1991, Swindell *et al* 1991, Swindell 1991, Radcliffe *et al* 1993, Bissonnette *et al* 1994, Jaffray *et al* 1995a, 1995b, Bissonnette *et al* 1997a, 1997b, Drake *et al* 2000). These efforts, and those of others, stimulated the widespread commercialization of camera-based EPIDs starting from the late 1980s.

A variety of interesting variations on the basic camera-based system illustrated in figure 4 have been developed. One approach, which was commercially available for a time, involved the use of fibreoptic bundles to transport the light emitted by the metal plate/phosphor screen converter to a camera, eliminating the mirror and lens and thus reducing the bulk of the

Table 1. Summary of technologies explored in electronic portal imaging systems. The technologies are divided into optical and non-optical systems and are further divided on the basis of whether they function as a one-dimensional or a two-dimensional detector. For each device, a general description is given along with the nature of the x-ray converting material, the institution(s) where the development originated, and informative references, including pertinent review articles. Further references are included in the main text.

Description of system	X-ray detector	Originating Institution	References
Optical systems			
Two-dimensional area detectors			
Camera with scintillator			
+ x-ray image intensifier	Fluorescent screen	Chalmers University of Technology	(Wallman 1958; review: Munro 1995, 1999)
+ mirror + lens	Fluorescent screen	NCI, Bethesda	(Andrews 1958; review: Webb 1993, Munro 1995, 1999, Herman 2001)
+ mirror + lens	Metal plate + fluorescent screen	University of Goteborg	(Benner 1962; review: Boyer 1992, Webb 1993, Munro 1995, 1999)
+ fiber-optic image reducers	Metal plate + fluorescent screen	Washington University	(Wong 1990; review: Boyer 1992, Webb 1993)
+ mirror + segmented scintillator	Metal plate + segmented CsI(Tl) crystals	Royal Marsden	(Mosleh-Shirazi 1998)
+ mirror + transparent scintillator	Transparent CsI(Tl) crystal	University of Tennessee	(Zeman 1998, Sawant *et al* 2002)
Indirect detection, active matrix flat-panel array	Metal plate + GdO_2S_2:Tb screen	University of Michigan	(Antonuk 1991a, 1992a, 1998a; review: Boyer 1992, Munro 1995, 1999, Antonuk 1998b)
One-dimensional scanning detectors			
Scintillation crystal-photodiode detector	$ZnWO_4$ crystals	Royal Marsden	(Morton 1988, Morton 1991; review: Boyer 1992, Webb 1993)
Scintillation crystal-photodiode detector	CsI(Tl) crystals	Royal Marsden	(Symonds-Tayler 1997)
Non-optical systems			
Two-dimensional area detectors			
Gas electron multiplier	Metal plates	Karolinska Institutet	(Brahme 2000, Ostling 2000, Iacobaeus 2001)
One-dimensional scanning detectors			
High-voltage rectifier diode array	Pb strip + diodes	Johns Hopkins	(Taborsky 1982, Lam 1986, 1987; review: Boyer 1992, Webb 1993)
Photovoltaic detector array	CdTe diodes	RMD + MGH	(Entine 1992, 1993)
Matrix liquid ionization chamber	Metal plate + iso-octane	NKI	(Meertens 1985, van Herk 1991; review: Boyer 1992, Webb 1993, Munro 1995, 1999, Herman 2001)
Kinestatic charge detector	∼100 atm Xe gas	University of Tennessee	(DiBianca 1997, Samant 1999.)

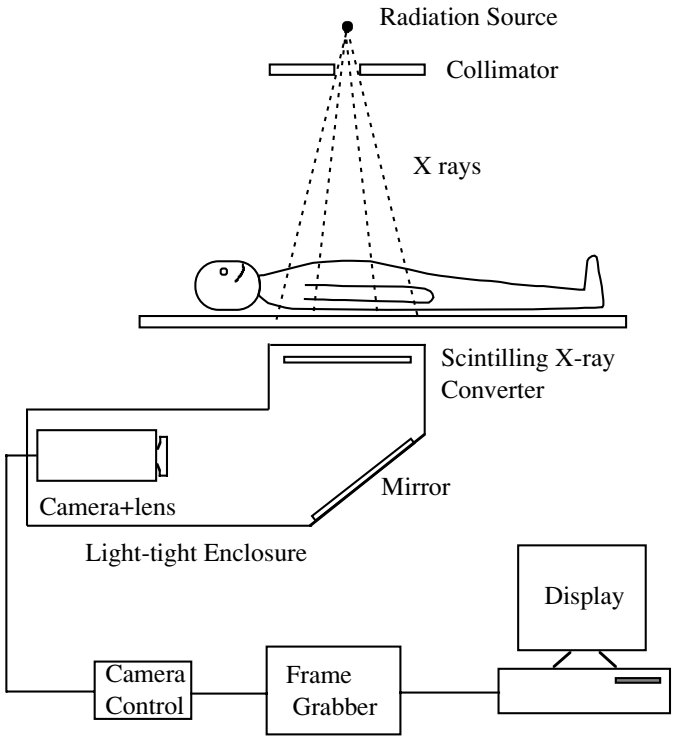

Figure 4. Schematic illustration of a camera-based EPID with the x-ray detector (a phosphor screen) optically coupled to the camera using a mirror and lens.

detector (Wong *et al* 1990, 1993). The merits and disadvantages (including spatial distortions and non-uniformities created by the fibreoptic bundles) of this approach are discussed in Webb (1993) and Boyer *et al* (1992). Currently, efforts are being made to significantly increase the efficiency of x-ray detection (and hence the detective quantum efficiency) of camera-based systems by replacing the phosphor screen with converters such as a thick, transparent CsI(Tl) crystal (Zeman *et al* 1998, Sawant *et al* 2002) or thick, segmented CsI(Tl) crystals (Mosleh-Shirazi *et al* 1998a, 1998b). These approaches are described in a later section.

Following its initial conception in 1987 by researchers at the University of Michigan and Xerox, PARC, an alternative two-dimensional optical technology for electronic portal imaging has recently been made commercially available after significant research and development. This technology, based on thin-film electronics of the sort used in active matrix, liquid crystal displays offers many advantages over existing commercial EPID systems and conventional radiotherapy film systems including significantly better image quality (Antonuk *et al* 1991a, 1992a, 1998a, 1998b). This approach is discussed in a later section.

In addition to these two-dimensional optical systems, another interesting optical system approach involves a one-dimensional detector array that is scanned across the field of view (Morton and Swindell 1987, Morton 1988, Morton *et al* 1991). This EPID, involving a double row of 2×64 zinc tungstate ($ZnWO_4$) crystals (each crystal being 5 mm $\times$ 5 mm $\times \sim$25 mm thick) to which photodiodes were attached, produced high quality images. The merits and disadvantages (primarily the relatively long irradiation times required per scan, $\sim$4 s) of the system are discussed in Boyer *et al* (1992). This system was used for portal imaging and transit dosimetry studies (Evans *et al* 1992, Hansen *et al* 1996). (A variant of the system

using a linear array of BGO crystals was designed for megavoltage CT (Lewis *et al* 1992).) A new version of this form of EPID, in which the $ZnWO_4$ crystals are replaced by a single row of 128 CsI(Tl) crystals (each crystal being 0.32 cm × 0.32 cm × 2.5 cm thick) has been developed (Symonds-Tayler *et al* 1997). This new system offers increased light yield and a better signal-to-noise ratio and is being used for scatter and transit dosimetry studies (Spies *et al* 2000, Evans *et al* 2000).

While the bulk of efforts to develop optical EPIDs have been directed toward two-dimensional systems, this has thus far not been the case for non-optical systems. Several non-optical systems developed in the early 1980s were based on a scanning linear array of silicon diodes (Taborsky *et al* 1982, Lam *et al* 1986, 1987). The largest such system consisted of 256 high-voltage rectifier diodes (each diode being 0.5 mm thick) arranged in a single row with a 2 mm spacing. An ∼1.1 mm layer of Pb was positioned over the diode array and the apparatus was scanned in 2 mm steps across the field. This system and its disadvantages (poor spatial resolution and very large doses required to generate a single image) are summarized in Boyer *et al* 1992. A similarly configured scanning system, developed by Radiation Monitoring Devices (RMD) and the Massachusetts General Hospital (MGH), utilized a linear array of 256 cadmium telluride (CdTe) photovoltaic diodes (Entine *et al* 1992, 1993). In a prototype system, each diode had a dimension of 2 mm × 2 mm × 2 mm. Compared to the silicon diodes of the previous system, these high atomic number, high density, relatively thick diodes offer significantly improved x-ray detection efficiency allowing the prototype system to provide high contrast images at significantly shorter scanning times. A scanning system based on a two-dimensional matrix ionization chamber was developed at the Nederlands Kanker Instituut (NKI) starting in the mid-1980s (Meertens *et al* 1985, Van Herk and Meertens 1987, 1988, Van Herk 1991, Van Herk *et al* 1992, Meertens *et al* 1990). This system has been commercially available since 1990 and, like the camera–mirror–lens-based systems using a metal plate/phosphor screen, produces images with significant amounts of clinically useful information. Both systems are more fully discussed in the next section.

Recently, two other novel, non-optical approaches for EPID design have been explored. A one-dimensional scanning system employing the kinestatic charge detection principle (DiBianca and Barker 1985) is under development at the University of Tennessee (DiBianca *et al* 1997, Samant *et al* 1999). In addition, a dual-energy (keV and MV) two-dimensional imager consisting of multiple gas-electron-multiplier detectors is under development at the Karolinska Institutet (Brahme *et al* 2000, Ostling *et al* 2000, Iacobaeus *et al* 2001). Each of these approaches is discussed in a later section.

3. First generation EPIDs in routine clinical use

As described above, among the many EPID technologies explored since the 1950s, only three approaches provided adequate amounts of clinically useful information and were sufficiently practical that they have been commercialized and widely adopted. Two of the approaches (camera–mirror–lens-based systems and the scanning matrix ionization chamber design) have been in widespread use for over a decade and represent the first generation of practical, commercially-available portal imaging technologies. These approaches are discussed in greater detail in the present section. A third approach (active matrix, flat-panel imagers), presently being introduced commercially, is described in the next section.

3.1. Camera–mirror–lens-based EPID systems using a metal plate/phosphor screen

As described previously, this approach has been under continuous, incremental development since the 1950s by a wide variety of investigators and institutions (Strandqvist and Rosengren

1958, Wallman and Stalberg 1958, Andrews *et al* 1958, Benner *et al* 1962, Baily *et al* 1980, Leong 1986, Shalev *et al* 1989, Munro *et al* 1987, 1988, 1990a, 1990b, Ezz *et al* 1991, Swindell 1991, Swindell *et al* 1991, Radcliffe *et al* 1993, Bissonnette *et al* 1994, Jaffray *et al* 1995a, 1995b, Bissonnette *et al* 1997a, 1997b, Drake *et al* 2000).

As illustrated in figure 4, the approach involves the use of an x-ray converter that is optically coupled to a camera by means of a mirror and a lens. The converter consists of a flat metal plate (typically an ∼1 to 1.5 mm copper, steel or brass plate) and a gadolinium oxysulfide (Gd_2O_2S:Tb) phosphor screen. The metal plate serves to convert incident primary x-rays into high energy electrons, some of which escape the plate into the phosphor, as well as to block low-energy, scattered radiation which would otherwise reduce the contrast of the imaging system. The phosphor serves to convert primary x-rays into high-energy electrons and transforms a fraction of the energy of the high-energy electrons passing through it into light. Some of the light diffuses through the screen, exiting on the mirror side. The camera and lens serve to capture a fraction of this emerging light and transform it into a video signal that is then sent to other hardware for digitization, processing, display and archiving. It is estimated that, depending on the thickness of the phosphor and the energy of the radiotherapy beam, on the order of only ∼2–4% of the incident x-rays interact and generate measurable signal in such systems (Herman *et al* 2001).

Given the large amounts of radiation associated with radiotherapy treatments, the electronics of the camera would quickly degrade if they were routinely exposed to the direct beam. For this reason, a mirror set at a 45° angle serves to direct the light out of the radiation field towards the camera. The lens serves to collect a fraction of the light emitted by the phosphor and focus it on the surface of the camera sensor. The optical components are enclosed in a light-tight housing to exclude light signal from sources other than the phosphor.

A major advantage of this approach is that the converter can cover all (or at least a very large fraction) of the portal field and the camera can sense the light signal from the entire converter simultaneously. Consequently, all of the radiation passing through the patient and incident upon the converter has the potential of generating signal in the camera and clinically useful images can be produced with as few as a couple of monitor units. A secondary, though important, practical advantage is that such systems can be assembled from relatively common, commercially available components. As a result, the system has been made available by a number of manufacturers (Munro 1995, Herman *et al* 2001). Pictures of commercial camera-based EPIDs are shown in figure 5.

One disadvantage of this approach is that the optical components and their light-tight housing are relatively bulky and present an encumbrance in the vicinity of where the therapists set up the patient. Moreover, mounting such systems on treatment machines with beam stoppers presents practical problems. The major disadvantage of the approach is that the optics of the system only allow those light photons emerging from the phosphor within a small cone subtended by the lens of the camera to generate signal in the camera (Munro 1995). As a result, only 0.1–0.01% of the light emerging from the phosphor reaches the sensor of the camera (Munro 1995)—an effect which reduces image quality as explained below. A fraction of the light that fails to reach the camera causes another image degrading effect. As described elsewhere (Munro *et al* 1998b, Munro 1999), some of the light emitted by the screen can reflect from the mirror so as to re-scatter from the phosphor screen and reach the camera. This signal then appears to have come from one part of the screen when, in fact, it originated from another part. This spurious signal, known as glare, can be more than 25% of the total measured signal, reducing contrast and complicating efforts to use the imager information for quantitative purposes such as transit dosimetry (Heijmen *et al* 1992, 1995).

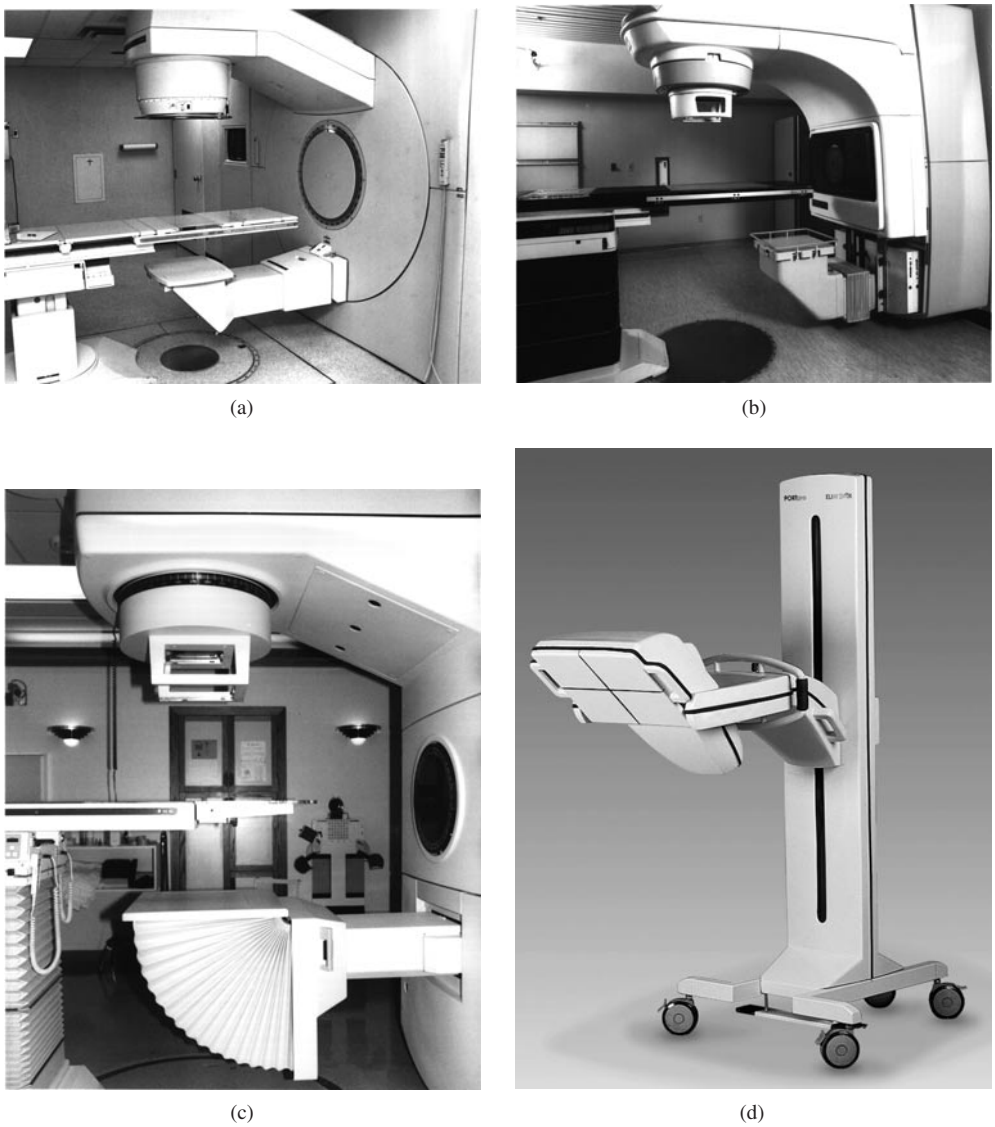

(a) (b)

(c) (d)

Figure 5. Photos of several commercial camera–mirror–lens-based systems using a metal plate/phosphor screen. Three systems mounted on a treatment machine: (a) Elekta 'iView' system (formerly sold by Philips and Elekta-Philips). (b) Cablon 'Theraview' system (formerly sold by Infimed)—shown in the retracted position when not in use. (c) Siemens 'Beamview' system. One system mounted on a stand like those used for film cassettes: (d) Eliav 'PORTpro' system. Illustrations for (a) and (c) are taken from Munro (1995) (reprinted with permission from Harcourt). Technical specifications of these systems are listed in Herman *et al* 2001.

The effect on image quality of the low light collection efficiency of the optical chain of camera-based EPIDs has been clearly elucidated through an analysis of the imaging situation (Bissonnette *et al* 1997b). This analysis is based on the cascaded systems formalism described in Cunningham *et al* (1994). In this formalism, an x-ray imager is represented by a series of 'stages' through which the imaging quanta pass. The stages may be of two types: (i) a *gain* stage in which the number or statistical distribution of imaging quanta changes (e.g.

incident x-rays interacting and creating high-energy electrons) and (ii) a *spreading* stage in which some physical process causes blur in the image (e.g. the scattering of light quanta in a phosphor screen). The physical transfer properties of these stages are quantified in terms of gain, spreading and noise parameters. For a given stage, the average number of imaging quanta per incident x-ray is given by the product of the gains up to and including that stage—a concept which is further generalized to the spatial frequency domain in the formalism. In a simple interpretation, the stage that has the lowest cumulative gain is said to be the 'quantum sink'. For a given x-ray imaging system, the stage at which the incident x-ray quanta interact in the converter (typically the first stage) is considered the 'primary' quantum sink (also called the x-ray quantum sink). The cumulative gain of this stage (given simply by the x-ray quantum detection efficiency) sets an absolute upper limit on the magnitude of the DQE. However, if the lowest cumulative gain occurs in a later stage, this represents a 'secondary' quantum sink and the magnitude of the DQE will be further reduced. In Bissonnette's analysis (Bissonnette *et al* 1997b), it is shown that the DQE performance of camera–mirror–lens-based EPID systems using a metal plate/phosphor screen is limited at lower frequencies (less than 0.25 cycles/mm) by both the primary quantum sink and by a secondary quantum sink in the number of detected optical quanta while performance at higher frequencies is limited by this secondary quantum sink.

Considerable empirical and theoretical research has been directed toward optimizing the performance of conventional camera–mirror–lens-based EPID systems. While this topic is adequately covered elsewhere (Webb 1993), a few efforts merit brief mention. For example, variations in the thickness or geometry of the metal plate and/or the phosphor screen have been studied in order to understand the effect upon DQE (Munro *et al* 1990b, Radcliffe *et al* 1993, Wowk *et al* 1993, 1994, Jaffray *et al* 1995a, Bissonnette *et al* 1997a). The situation is complicated (Herman *et al* 2001): thicker metal plates stop more x-rays but do not necessarily lead to more electrons entering the phosphor; thicker phosphor screens stop more x-rays and generate more light signal but degrade spatial resolution. In addition, the use of a large aperture lens improves the optical transfer efficiency (Munro *et al* 1990b) but such large lenses introduce spherical aberrations (which reduce spatial resolution) and distortion, among other effects (Herman *et al* 2001). An alternative strategy to partially compensate for poor light collection efficiency involves the reduction of system noise so as to improve the signal-to-noise ratio. This has been explored through extended integration of the light signal on the sensor of the camera (as opposed to digital averaging of frames acquired at the normal video rate) (Munro *et al* 1990b). Another noise reduction strategy involving the introduction of a cooled, low noise CCD camera improves imager performance to the point that the system is x-ray quantum limited at low spatial frequencies (Drake *et al* 2000). Yet another approach to improving the performance of camera–mirror–lens-based systems involves the incorporation of a high-gain camera (incorporating avalanche-multiplication) so as to reduce the relative importance of the camera noise (Pang and Rowlands 2000). As a result of such efforts, the maximum DQEs achieved for camera–mirror–lens-based EPID systems using a metal plate/phosphor screen are reported to be as high as $\sim$1%.

3.2. Scanning matrix ionization chamber EPID

Like the camera–mirror–lens-based systems described above, the EPID system based on a scanning matrix ionization chamber conceived and developed at the Nederlands Kanker Instituut (NKI) has been commercialized and widely adopted. Compared to camera-based systems whose development spanned more than three decades prior to the introduction of the first commercial systems in the late 1980s, the NKI system was developed over a relatively brief period in the 1980s prior to becoming commercially available in 1990

(Meertens *et al* 1985, Van Herk and Meertens 1987, 1988, Van Herk 1991, Van Herk *et al* 1992, Meertens *et al* 1990).

The approach involves the use of a liquid ionization chamber formed by two planes of electrodes separated by a 0.8 mm gap. The gap is filled with a fluid (2,2,4-trimethylpentane) which acts as an ionization medium when the chamber is irradiated. Each electrode plane consists of 256 parallel wires spaced 1.27 mm apart. The electrodes on the two planes are oriented perpendicularly to each other thereby forming a matrix of 256 $\times$ 256 ionization cells that provide a detection area of 32.5 $\times$ 32.5 cm^2. In addition, a 1 mm thick plastoferrite plate positioned over the ionization chamber serves the same purpose as the metal plate in camera-based systems—to convert primary x-rays into high energy electrons, some of which escape into the ionization medium, and to block low-energy, scattered radiation. The ionization medium also serves to convert primary x-rays into high-energy electrons and, analogous to the phosphor screen in some camera-based systems, transforms a fraction of the energy of the high-energy electrons passing through it into a measurable (ion) signal. A high-voltage supply is used to apply a 300 V bias to each electrode individually on one of the planes (the high voltage plane). The electrodes on the other plane (the signal plane) are individually connected to electrometers. The entire imager consists of the matrix ionization chamber, a 256-channel high-voltage switching system, a 256-channel electrometer, and control electronics. The chamber and peripheral electronics can be packaged compactly, as shown in figures 6(a), (b) and (c).

Full resolution readout of the imager is achieved by applying the high voltage to each of the electrodes on the high voltage plane in succession (for about 20 ms) and recording the signal generated in each of the 256 electrodes—a process requiring about 5.5 s for readout of the full imager. A faster (but lower resolution) readout mode is accomplished through application of the high voltage to pairs of electrodes for 10 ms resulting in a 1.5 s readout time for the full imager. More recent systems operate at 500 V bias with 5 ms per electrode allowing a total readout time of 1.25 s (Herman *et al* 2001).

Important advantages of this system include the compactness of the detector, approaching that of a film cassette, and the lack of geometric distortions in the image. The most significant disadvantage of this approach is that the utilization of incident x-ray quanta is inferior to that of a true area detector since, for full-resolution readout, only a single electrode on the high voltage plane is switched on at a time. This undesirable situation is somewhat improved by the fact that the rate of ion recombination in the 2,2,4-trimethylpentane is, even in the absence of high voltage, relatively slow ($\sim$0.5 s). As a consequence, signal measured from any given ionization cell during the 5 to 20 ms application of high voltage contains information about x-ray interactions in the previous $\sim$0.5 s, improving the utilization of the incident x-ray quanta. Nevertheless, this effective integration time of $\sim$0.5 s is still short compared to the total image acquisition time and thus a significant amount of incident radiation generates no useful signal. As a result, while $\sim$1.5% of the incident x-rays interact in the plastoferrite plate and liquid ionization medium and generate measurable signal (Herman *et al* 2001), the DQE of the system is, at best, only on the order of 0.5% due to the signal loss in sampling (Van Herk 2001). Consequently, the total dose required to generate an image is larger than that for EPIDs incorporating true area detection. In addition, the sampling frequency of the detection elements of this system is lower than that for the other commercially-available EPIDs.

4. Active matrix, flat-panel imager (AMFPI) EPIDs

Following extensive research and development efforts at the University of Michigan, Xerox PARC and elsewhere starting in 1987 (Street *et al* 1990, Antonuk *et al* 1990a, 1990b, 1991a,

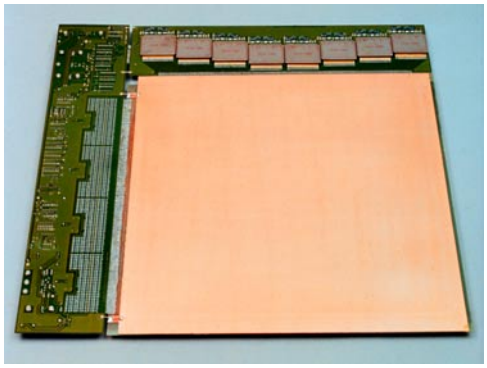

(a)

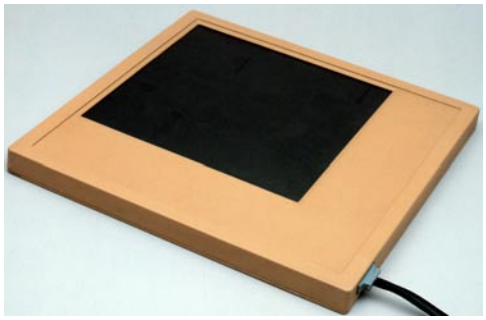

(b)

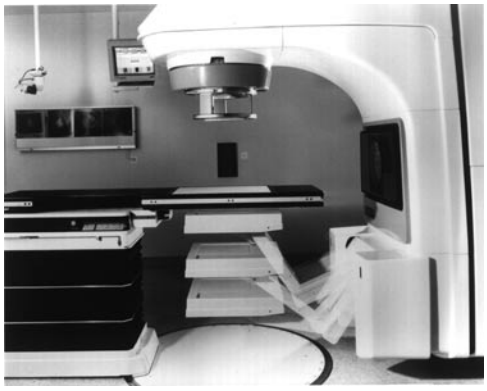

(c)

Figure 6. Photos of the matrix ionization chamber EPID design. (a) View of interior components. (b) Early packaging of system in a film-cassette-like housing. (c) Varian system mounted on a treatment gantry with the detector housing shown (by means of a multiple-exposure) in three imaging positions, taken from Munro (1995) (reprinted with permission from Harcourt).

1991b, 1991c, 1992a, 1992b, 1992c, 1992d, 1994, 1996, 1998a, 1998b, Boudry and Antonuk 1994, 1996, Bissonnette *et al* 1997a, Drake *et al* 1997, Earnhart and Chaney 1997, Munro *et al* 1998a, El-Mohri *et al* 1999, 2001), indirect detection active matrix, flat-panel EPIDs became commercially available for the first time in 2000. (Extensive development of the technology for diagnostic imaging has also occurred at Michigan, Xerox and elsewhere, but is a topic beyond the scope of the present review.) Details about the technology, its operation, and its advantages for portal imaging are given in this section which derives partly from earlier, more extensive descriptions of the technology, its properties and performance (Antonuk *et al* 1998b). Further detailed descriptions of this imaging technology and of the semiconductor technologies that underlie it may be found in Street (1991, 2000) and Antonuk *et al* (1992a, 1998a).

4.1. General description of AMFPIs

Active matrix, flat-panel imagers (AMFPIs) may be considered to consist of the following subsystems: (a) a large area, pixelated array; (b) an overlying x-ray converter; (c) an electronic

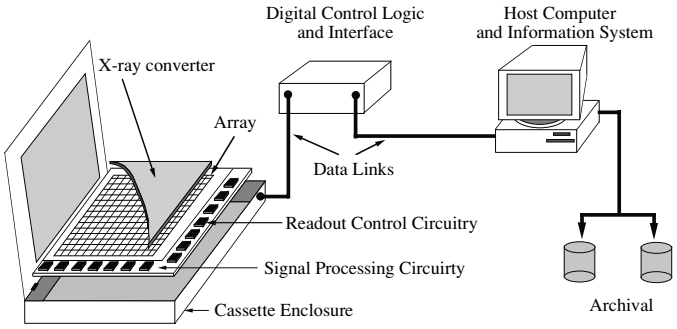

Figure 7. Schematic illustration of the elements of an active matrix, flat-panel imager (AMFPI). Adapted from Antonuk *et al* (1998b) (reprinted with permission from AAPM).

acquisition system which controls the operation of the array and extracts and processes analog signals from the array pixels and (d) a host computer and information system which sends commands to, and receives digital pixel data from the acquisition system as well as processes, displays, and archives the resulting digital images. These elements are illustrated schematically in figure 7.

The distinguishing feature of AMFPI technology is the array which consists of an ∼1 mm thick glass substrate on which thin-film electronic circuits reside. These circuits are created through a series of semiconductor processing steps involving plasma enhanced, chemical vapor deposition (PECVD), etching and passivation—typically involving 5–10 sets of photolithographic masks. A schematic illustration of a portion of an array and its external, peripheral control and processing circuits is given in figure 8. By definition, each pixel in an active matrix array incorporates a thin-film switch connected to some form of capacitive element. The pixels are organized in a two-dimensional grid and the conductivity of the pixel switches is controlled through variation of the voltage of control lines with each control line connected to all of the pixel switches in a single row. (The control lines are often called *gate control* lines for array designs incorporating a pixel switch consisting of a thin-film transistor—see below.) During imager operation, the pixel switches are generally kept non-conducting so that charge generated directly or indirectly by incident radiation interacting in an overlying x-ray converting material is integrated in the capacitive element of each pixel. Readout of these imaging signals from the capacitive elements is accomplished by rendering the pixel switches conducting. Typically, one row of pixels is read out at a time for maximum spatial resolution, although multiple rows can be read out at a time for faster readout at lower resolution. When the pixel switches along a given row are made to conduct, imaging signals stored in the pixels are sampled by external peripheral electronics by means of *data* lines, with each data line connected to all the pixel switches in a given column. The action of reading out the pixels also reinitializes them—although additional initialization steps may be required depending on the type of switch and the nature of the converter. The general organization of these imaging arrays is parallel to that of active matrix liquid-crystal displays (AMLCDs, commonly used for laptop computers) which also employ a two-dimensional 'active matrix' of thin-film switches to control the output of light allowing the display of images.

4.2. Description of different AMFPI designs for portal imaging

The pixel switches thus far employed for the majority of AMFPI designs are thin-film transistors (TFTs) fabricated from hydrogenated amorphous silicon (a-Si:H). (While

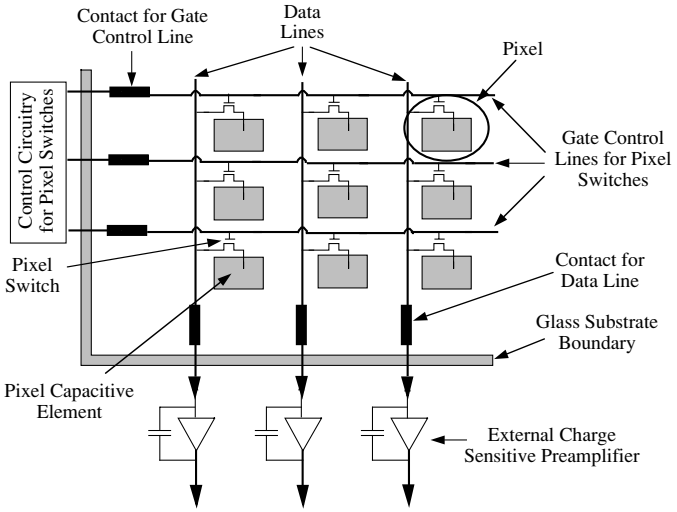

Figure 8. Schematic illustration of a corner of an indirect or direct detection active matrix, flat-panel imaging array illustrating the matrix addressing scheme of such designs. Also illustrated is external peripheral control circuitry that is connected to the array via peripheral contacts—one contact for each gate control line and each data line. This circuitry controls the conductivity of the pixel switches and amplifies the pixel signals. As an example, the pixel switches are represented as TFTs but diode-based switches are also used in some diagnostic imager designs. The capacitive element depicted for each pixel in the figure corresponds to a photosensor for an indirect detection array and a storage capacitor for a direct detection array. Adapted from Antonuk *et al* (1998b) (reprinted with permission from AAPM).

considerable effort has also been devoted to the development of pixel switches based on a single, or a pair of a-Si:H diodes, this has thus far been restricted to some imagers designed for diagnostic radiographic imaging.) Concerning the conversion of incident x-ray energy into charge stored in the capacitive element in each pixel, two general approaches can be distinguished based on how this imaging signal is generated and stored in the pixels. Indirect detection AMFPIs use an x-ray converter consisting of a combination of a metal plate and a scintillator—with the scintillator positioned directly over the photosensor integrated into the array. In this approach, some of the radiation-induced light escapes the scintillator in the direction of the photosensor. Light entering the photosensor is converted into electron–hole pairs, one electron–hole pair per detected light photon. The structure of the photosensor also forms the capacitive element in each pixel where this signal is stored until readout. Direct detection AMFPIs use an x-ray converter consisting of a combination of a metal plate and a photoconductor—with the photoconductor electrically coupled to a separate capacitor built into each pixel. In this approach, the radiation generates electron–hole pairs in the photoconductor and this imaging signal is stored in the pixel capacitors until readout.

4.3. Indirect detection active matrix flat-panel EPIDs and their advantages

Thus far, commercial EPID systems incorporating active matrix flat-panel arrays are based solely on the indirect detection approach. In these systems, the photosensor is a discrete a-Si:H photodiode located in each pixel. (Recently, a continuous a-Si:H photodiode structure has been developed that increases the optical fill factor of the arrays, i.e. the fraction of the pixel that is sensitive to light from the scintillator (Mulato *et al* 2001). Although such structures

could conceivably appear in commercial megavoltage imaging arrays in the future, increasing the optical fill factor is generally an issue only for arrays designed for considerably higher resolution applications.) The scintillator incorporated in present commercial systems is a phosphor screen, although columnar CsI(Tl) is likely to be explored for portal imaging in the future. Columnar CsI(Tl) is popular for diagnostic imaging applications as its needle-like structure assists in confining the lateral spread of light as the thickness of the scintillator increases, thus preserving spatial resolution. Figures 9(a) and (b) schematically illustrate side views of pixels incorporating each of these scintillator types. In addition, for the TFT + photodiode array designs used for portal imaging, the action of reading out the pixels also reinitializes them.

Specifications of commercial EPIDs based on active matrix technology are given in table 2. The first commercial system was introduced by Varian Medical Systems in 2000 and offers a 30×40 cm^2 detection area. (An earlier commercial alpha-prototype produced by this company was based on an array with a 26×26 cm^2 detection area developed earlier for radiotherapy research by Michigan and Xerox, PARC (Antonuk *et al* 1995, 1998a).) A second commercial EPID based on the same technology was introduced by Elekta Oncology Systems in mid-2001 and offers a 41×41 cm^2 detection area. Finally, a prototype imager based on this technology from Siemens Medical Systems with a 41×41 cm^2 detection area is presently undergoing clinical evaluation. Pictures of two of these imagers are shown in figure 10. Based on studies of a research prototype of similar design (El-Mohri *et al* 2001), the DQE of such systems when operated with an $\sim$133 mg cm^{-2} phosphor screen is anticipated to be slightly greater than 1% at 6 MV.

Indirect detection AMFPIs offer a variety of advantages for the portal imaging application. This solid state technology facilitates the creation of compact detectors (as illustrated in figure 10) offering real-time, digital readout. The technology also allows the creation of very large-area arrays which dwarf the largest commercially available, pixel-based crystalline-silicon imaging structures, namely, charge-coupled device (CCD) arrays with a sensitive area of $\sim 8 \times 8$ cm^2. By comparison, monolithic active matrix flat-panel arrays as large as 41×41 cm^2 have thus far been produced (table 2). If required by the application, even larger detectors should be possible, for example, through tiling of two or four arrays (Colbeth *et al* 1997). The arrays and their acquisition systems may be designed to provide both radiographic readout (i.e. capture of single frames) or fluoroscopic readout (e.g. up to 30 frames per second (Antonuk *et al* 1993)). The signal response of the pixels is highly linear (Antonuk *et al* 1998a) and the technology can be configured for dosimetric measurements (El-Mohri *et al* 1999, McCurdy *et al* 2001). Moreover, the a-Si:H TFTs and photodiodes are highly resistant to radiation damage (Antonuk *et al* 1990b, Boudry and Antonuk 1994, 1996)—even at the very high doses to which a portal imager could be exposed (in excess of 10^4 Gy per year). Of course, attention must also be paid to the issue of radiation damage to the readout circuits located around the periphery of the arrays.

Perhaps one of the most important advantages of AMFPI technology for portal imaging is the high degree of image quality. For example, given: (a) that the array photodiodes are in close proximity to the scintillator; (b) that a large fraction of the pixel area is occupied by the photodiode for arrays designed for portal imaging; (c) the high efficiency of conversion of light entering the photodiodes into electron-hole pairs and (d) the high efficiency of readout of the signal from the pixels; then AMFPI-based EPIDs are capable of using on the order of 50% of the light emitted from the scintillator. This value is several orders of magnitude larger than optical transfer efficiencies for camera–mirror–lens-based systems. Consequently, secondary quantum sinks in the number of detected optical quanta, which limit the performance of camera-based EPIDs, are absent in AMFPI-based EPIDs allowing this

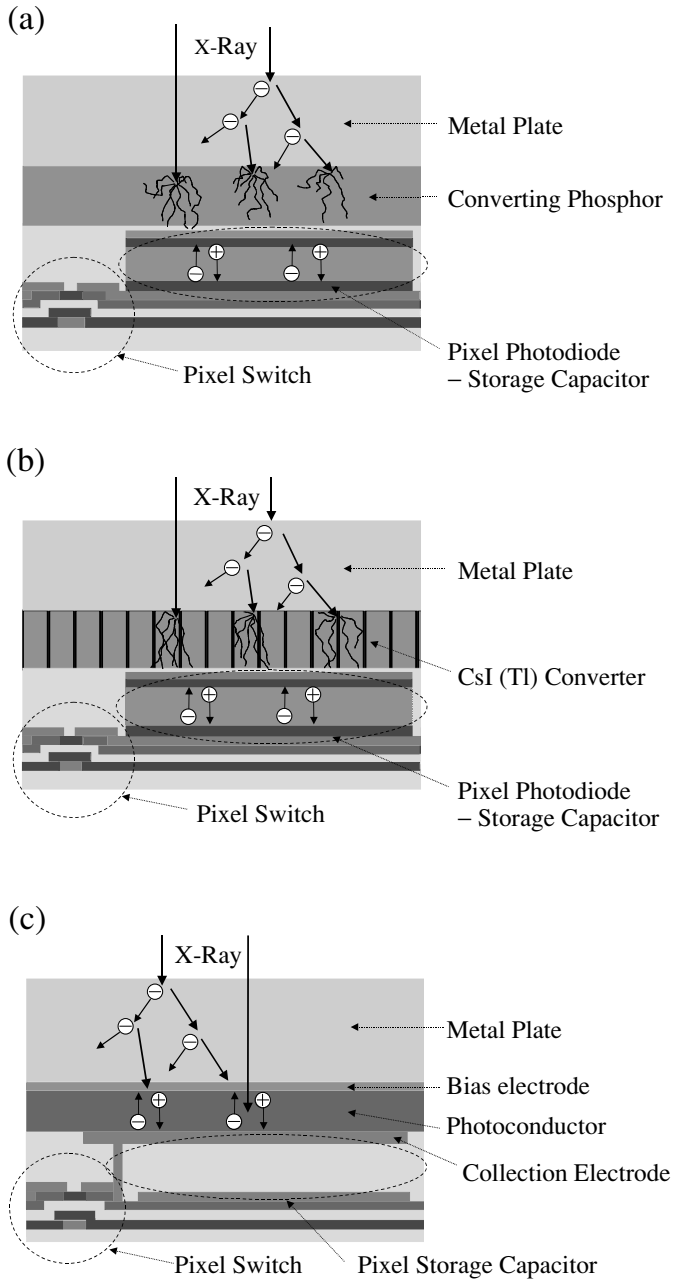

Figure 9. Schematic illustration (not to scale) of x-ray detection in an AMFPI for (a) and (b) indirect detection using a phosphor and a columnar CsI(Tl) scintillator, respectively; and (c) direct detection of the incident radiation. In each case, the x-ray converter over a single pixel is illustrated. Taken from Antonuk *et al* (1998b) (reprinted with permission from AAPM).

technology to offer x-ray quantum limited imaging (Munro and Bouius 1998a, El-Mohri *et al* 2001). The close proximity of the photodiodes to the scintillator also sharply limits or eliminates glare in AMFPIs—a problem for camera–mirror–lens-based systems. Moreover,

Table 2. Specifications of commercial imagers based on indirect detection, active matrix flat-panel imaging technology. Information not available at the time of publication is so indicated. For the Varian system, the asterisk refers to the fact that the pixel format and pixel-to-pixel pitch of the array are actually 1024 × 768 pixels and 392 μm, respectively, while the system is presently configured to provide readout at a lower resolution.

Company	Varian Medical Systems	Elekta Oncology Systems
Product	PortalVision aS500	*i*ViewGT
Commercial availability	2000	2001
Detector area	40.14 × 30.11 cm^2	40.96 × 40.96 cm^2
Array format	Monolithic array	Monolithic array
Pixel format	512 × 384*	512 × 512
Pixel pitch	784 μm*	800 μm
Maximum image acquisition rate	10 frames per second (frames averaged in hardware)	3 frames per second
Image display and storage rate	2 seconds per image	∼0.3 seconds per image
Digitization	14 bits	16 bits
Metal plate	1 mm Cu	1 mm Cu
Scintillator	133 mg cm^{-2} Gd_2O_2S:Tb	Gd_2O_2S:Tb
Miscellaneous	Neutral density filter	n/a

preliminary studies comparing AMFPI-based and matrix-ionization-chamber-based EPIDs strongly suggest superior image quality from the AMFPIs (Van Herk 2001). Finally, an observer-based contrast-detail study comparing an AMFPI-based EPID and portal film systems (the current gold standard in portal imaging) indicate that AMFPIs offer performance superior to that of a conventional portal imaging film system (Antonuk *et al* 1998). Moreover, this was true even when images made with the AMFPI used less radiation than the film system. Furthermore, in a comparison between the AMFPI and the EC-L portal film system, the levels of performance were found to be similar, although this was true only over a very narrow range of exposure in which the EC-L film was neither under- nor over-exposed. These early studies suggest that AMFPIs may offer considerable improvements in portal imaging quality compared to present commercial systems.

An illustration of the image quality to be expected from an AMFPI-based EPID is shown in figure 11. (Images from earlier EPID systems appear throughout the literature, e.g. in the prior reviews cited in section 1.3.) The images in figure 11 were obtained radiographically and are of the pelvic region of a single patient (Antonuk *et al* 1998a). Single exposure images obtained at 6 and 15 MV at exposures of 4 and 3 MU are shown in figures 11(a) and (b), respectively. In addition, figures 11(c) and (d) show double-exposure AMFPI images taken at 6 and 15 MV, respectively, each of which consists of a pair of images captured in the presence and absence of a shaped collimation block, and then digitally added. The double-exposure images were acquired at the lowest available dose setting (1 MU for each individual image). For purposes of comparison, images of the same patient taken with a standard radiotherapy film cassette, double-exposed in the conventional manner, at doses corresponding to those used in routine clinical practice are shown for 6 and 15 MV in figures 11(e) and (f), respectively. The image processing of the AMFPI images was minimal and consisted of simple gain and offset corrections, filtering to eliminate the distracting influence of pixel and line defects, and window and level adjustments of the digital data. The films were digitized and subject to more extensive processing in order to maximize the presentation of information content that would otherwise be obscured due to the logarithmic response of the film.

(a)

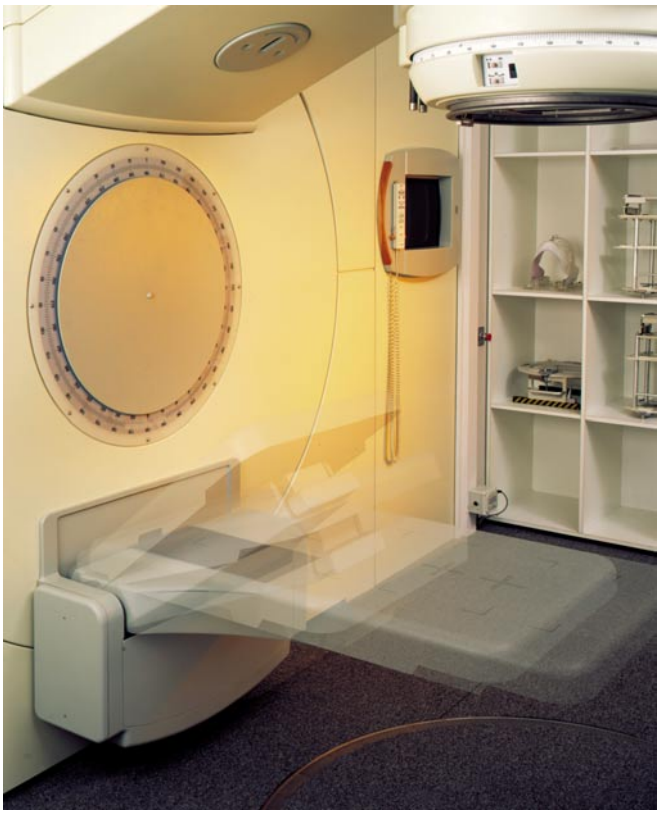

(b)

Figure 10. Photos of two indirect detection, active matrix flat-panel systems. (a) PortalVision aS500 from Varian Medical Systems. (b) *i*ViewGT from Elekta Oncology Systems with the detector box shown (by means of a multiple-exposure) in various stages of retraction toward the treatment gantry. See table 2 for related design specifications. Photos courtesy of Ed Shapiro and Kevin Brown.

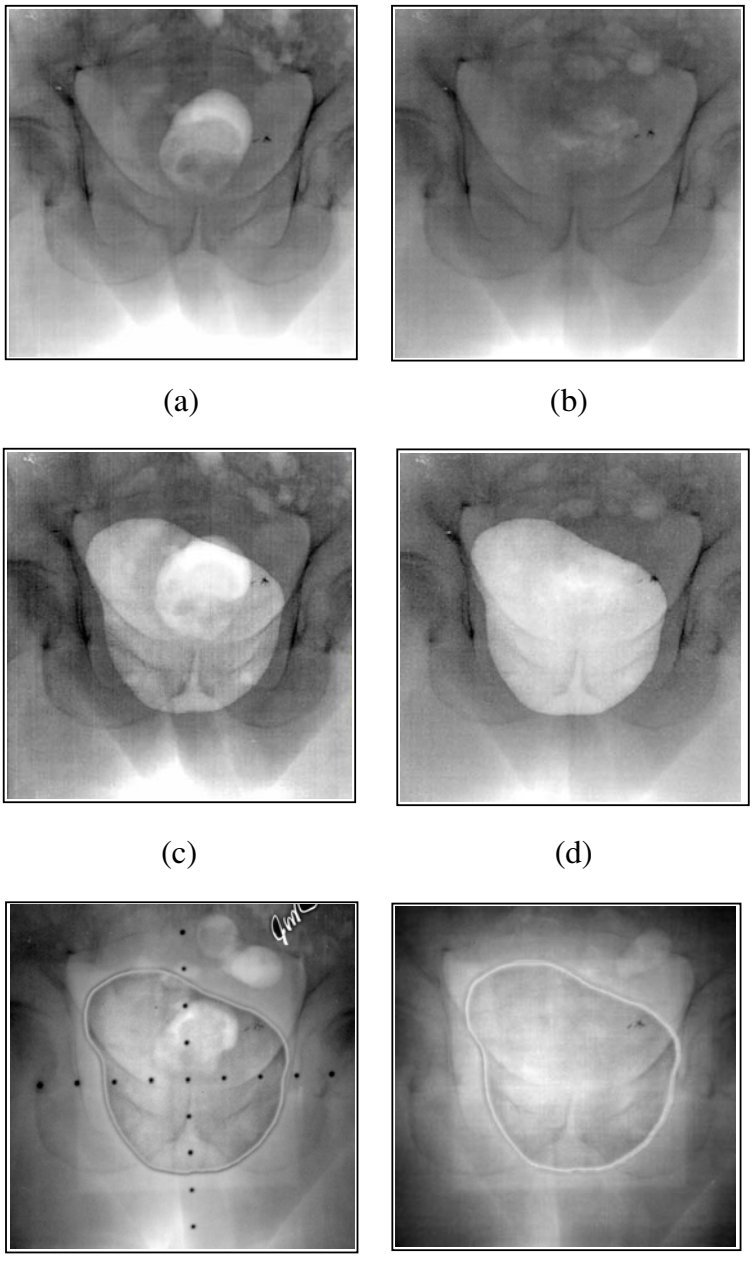

Figure 11. Radiographic images acquired in the pelvic region of a patient (Antonuk *et al* 1998a; reprinted with permission from Elsevier Science). The images were acquired with a prototype indirect detection AMFPI under conditions of (a) single exposure—6 MV, 4 MU; (b) single exposure—15 MV, 3 MU; (c) double-exposure—6 MV, 1 + 1 MU (i.e. 1 MU with a shaped collimation block and 1 MU without the block in place); and (d) double-exposure—15 MV, 1 + 1 MU. The AMFPI incorporates a 508 μm pitch, 512 $\times$ 512 pixel array and uses a 1 mm Cu metal plate and a 70 mg cm^{-2} Gd_2O_2S:Tb phosphor screen. Double-exposure images acquired with a standard radiotherapy film cassette under conditions of (e) 6 MV, 3 + 3 MU and (f) 15 MV, 4 + 4 MU.

The single exposure images obtained with the AMFPI system (figures 11(a) and (b)) demonstrate excellent contrast resolution and provide sufficient anatomical detail to allow confident localization. Even at 15 MV, image quality is only somewhat reduced compared to 6 MV. Moreover, despite the minimal doses used in the AMFPI double-exposure images (figures 11(c) and (d)), they compare quite favourably with the film images (figures 11(e) and (f)) that were taken at higher doses. Images such as those shown in the figures give an indication of the quality provided by the current gold standard, film, and the potential of the relatively recent AMFPI EPID technology.

4.4. EPIDs based on direct detection active matrix flat-panel technology

Although commercially available active matrix flat-panel EPIDs are exclusively based on indirect detection, it is likely that direct detection AMFPIs will be thoroughly explored for portal imaging given their commercial availability for diagnostic imaging. In the direct detection approach, a continuous layer of photoconductive material is deposited over the surface of the array (Zhao and Rowlands 1995). In this case, each pixel has an auxiliary storage capacitor connected to the pixel switch as well as to a collection electrode that serves to gather signal from the photoconductor. A likely configuration for the portal imaging application is illustrated in figure 9(c) which schematically illustrates a side view of a direct detection pixel incorporating an overlying metal plate and continuous photoconductive layer.

Thus far, the only photoconductor used in commercial AMFPIs for diagnostic imaging is amorphous selenium (a-Se) with thicknesses up to $\sim$1000 μm (Tsukamoto *et al* 1999, Adachi *et al* 2000, Choquette *et al* 2000). (Other materials such as lead iodide (PbI_2), mercuric iodide (HgI_2), and cadmium telluride (CdTe) are also under examination for diagnostic imaging (Street *et al* 2001, Adachi *et al* 2000).) Given that 1000 μm of a-Se would have an estimated x-ray quantum detection efficiency of $\sim$3% for a 6 MV beam, the use of this material in a direct detection AMFPI for portal imaging would be of interest. Early studies of the use of a-Se for portal imaging have been reported (Falco *et al* 1998, Lachaine and Fallone 1998, Lachaine *et al* 2001, Mah *et al* 1998, 1999, Pang *et al* 2001) and interest in this material is likely to continue.

5. Contemporary research toward improving EPID performance

In recent years, a number of efforts have been made to explore new technologies for electronic portal imaging devices or attempt to address weaknesses in existing technologies (Mosleh-Shirazi *et al* 1998a, 1998b, Zeman *et al* 1998, Sawant 1999, Sawant *et al* 2002, DiBianca *et al* 1997, Samant *et al* 1999, Brahme *et al* 2000, Ostling *et al* 2000, Iacobaeus *et al* 2001). In this section, we shall briefly outline these ongoing research activities which are largely focused on improving the efficiency of detection of the incident primary x-ray radiation.

One particular direction of these research efforts is to significantly increase the x-ray quantum detection efficiency of camera–mirror–lens-based EPID systems from the present low levels of $\sim$2–4% (Herman *et al* 2001). Such an effort is being carried out by the Joint Department of Physics, Institute of Cancer Research and Royal Marsden NHS Trust and involves replacing the phosphor screen with a scintillator consisting of a two-dimensional array of CsI(Tl) elements (Mosleh-Shirazi *et al* 1994, 1998a, 1998b). This system has the same optical geometry as conventional camera-based systems, as illustrated in figure 12(a). The x-ray converter has an area of 45 $\times$ 60 cm^2 and consists of 100 modules. Each module comprises a 15 $\times$ 20 array of optically isolated CsI(Tl) detector elements. Each element is 3 mm $\times$ 3 mm $\times$ 10 mm thick (giving an x-ray quantum detection efficiency of $\sim$18% at 6 MV)

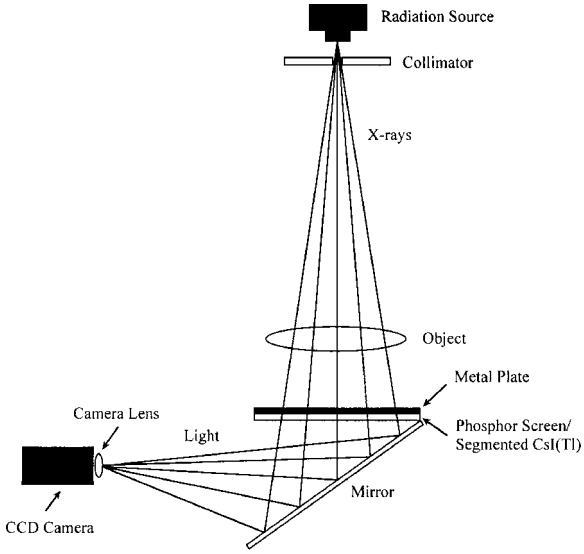

(a)

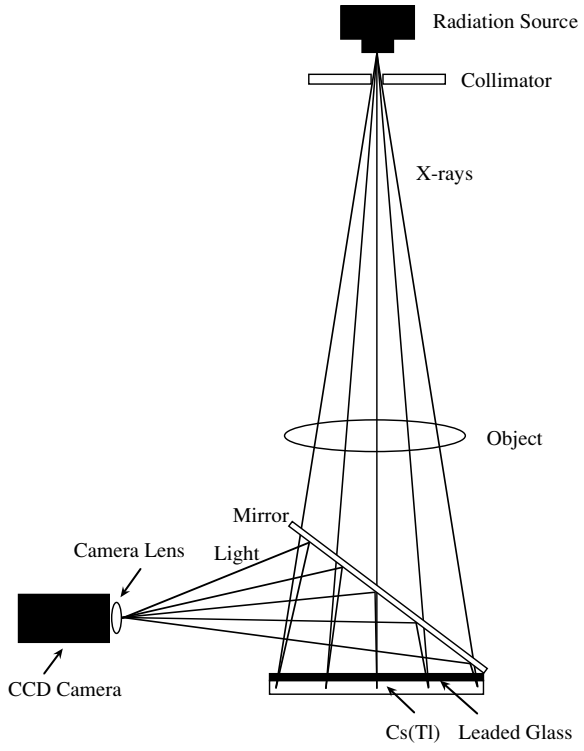

(b)

Figure 12. Schematic illustrations of the optical elements for various geometries used for camera-based EPID systems. (a) Geometry commonly used for conventional camera–mirror–lens-based systems using a metal plate/phosphor screen or a metal plate/segmented CsI(Tl) converter. (b) Geometry used for the camera-based system involving a thick CsI(Tl) scintillator under development at the University of Tennessee, adapted from Sawant *et al* (2002) (reprinted with permission from AAPM).

and is optically separated from neighbouring elements by 0.3 mm gaps filled with titanium dioxide-loaded epoxy resin. The modules are attached to a 3 mm thick aluminium plate. The converter is positioned 150 cm from the source providing an impressive 30×40 cm^2 field-of-view at the isocentre. In addition, each radiation pulse leads to a camera frame that is summed by a frame grabber. The system reportedly allows a 2 mm diameter structure of 1.3% contrast and an 18 mm diameter object of 0.125% contrast to be resolved at 6 MV with an $\sim 1 \times 10^{-2}$ Gy irradiation and provides a spatial resolution of $\sim$2 mm at the isocentre (Mosleh-Shirazi *et al* 1998b). The authors further report that the system is limited by a low optical-coupling efficiency and significant dark current in the CCD camera sensor—limitations which they indicate can be largely removed through the use of a cooled, large area CCD and a fast lens.

Another novel approach towards significantly increasing the use of the incident x-rays in camera–mirror–lens-based systems involves replacing the metal plate/phosphor screen with a lead-glass plate coupled to a thick, transparent CsI(Tl) scintillator (Zeman *et al* 1998, Sawant 1999, Sawant *et al* 2002). In this approach, the mirror–lens–camera combination is located on the same side as the x-ray source, as illustrated in figure 12(b), rather than on the opposite side as in conventional systems (figure 12(a)). A plate of $\sim$1 cm thick transparent lead-glass with an index of refraction matched to that of CsI(Tl) (1.79) is optically coupled to the front of the scintillator. This layer, having an x-ray absorption approximately equivalent to that of 1 mm of lead, serves to block the scattered radiation which would otherwise reduce the contrast of the system and serves to allow scintillator light to reach the camera. In addition to these primary functions, the lead-glass plate also converts some of the incident x-rays into high energy electrons which escape into the scintillator. The optics of the system are designed to allow light generated by all x-rays interacting along a given incident trajectory to be recorded at a single point on the camera sensor, as illustrated in figure 13. Since light emerging from the scintillator–lead–glass combination is subject to refraction, this optical result can be achieved by collecting the light emerging from the front of the scintillator by placing the camera sensor at an appropriate distance. In the small angle approximation, this distance is given by $\frac{D}{n}$, where D is the distance from the x-ray source to the scintillator and n is the index of refraction for CsI(Tl). The primary merit of this EPID design is that it allows the use of a thick scintillator (and thus increased use of the incident x-rays) without significant loss of spatial resolution due to spreading and scattering of light photons in the scintillator, as is the case for phosphor screens. Rather, the spatial resolution of the system is limited by a combination of the spread of the secondary radiation that produces the light photons and the limited depth of focus of the optics. One configuration that has been examined involved a 12.5 mm thick CsI(Tl) scintillator that provides an x-ray quantum detection efficiency of $\sim$25% (Sawant *et al* 2002). While the performance of this proposed system is still limited by a secondary quantum sink in the number of detected optical quanta (as for most camera-based systems), calculations suggest that the zero-frequency DQE would be as high as $\sim$11%. In addition, due to the need to place the mirror in front of the scintillator, the x-ray converter must be located further from the source thereby requiring a larger area detector in order to image a given field of view at the isocentre.

Another approach towards increasing the x-ray quantum detection efficiency for portal imaging involves the use of the kinestatic charge detection (KCD) technique originally developed for diagnostic imagers (DiBianca and Barker 1985). The KCD approach, illustrated in figure 14, involves the use of an x-ray detector that is scanned across the field of view. The detector consists of an x-ray detection volume and a signal collection volume. The design of the KCD system under development for portal imaging (DiBianca *et al* 1997, Samant *et al* 1999) closely parallels that of a previously developed high-pressure gas-based diagnostic

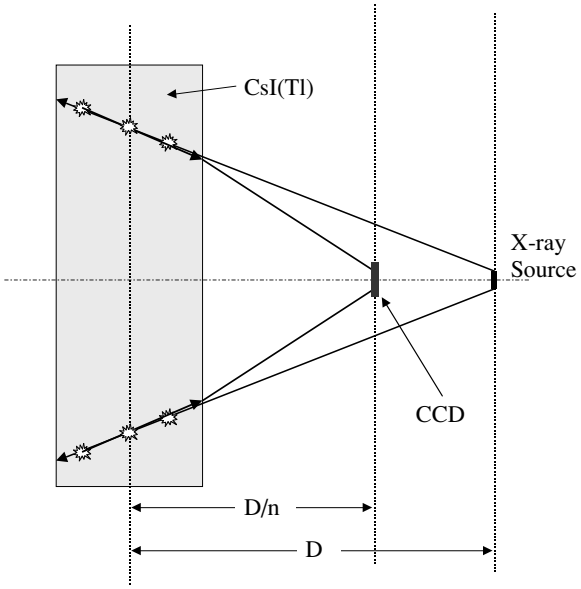

Figure 13. Schematic diagram illustrating an essential principle of the optics of the camera-based system under development at the University of Tennessee, corresponding to figure 12(b). In this diagram, the lead glass plate, the 45° mirror and the lens have been omitted for clarity of presentation. By gathering light emerging from the front of the CsI(Tl) scintillator on a camera sensor placed at a carefully chosen distance ($\frac{D}{n}$), light from x-rays interacting along a given incident trajectory is recorded at a single point on the sensor. Note that if the camera sensor were placed on the far side of the scintillator (as in conventional camera-based systems, figure 12(a)), the light from x-rays along a given trajectory would be focused along a line on the sensor, rather than on a point (Sawant *et al* 2002).

imager (DiBianca *et al* 1996). In the design, while the detection volume is continuous, the signal collection volume consists of a linear array of n discrete charge detection elements. Incident x-rays interact and generate charge in the detection volume. An electric field applied across this volume drives a portion of this charge toward the signal collection elements that serve to continuously produce a spatially discrete set of n signals that may be amplified and digitized. Central to the KCD technique is the fact that the detector is mechanically scanned at a speed equal and opposite to the signal charge drift velocity, in a direction perpendicular to that of the x-ray beam. As illustrated in figure 14(c), this procedure makes the secondary ionization cloud created by the interacting x-rays stationary relative to the coordinate system of the radiation source. Thus, for a given incident x-ray trajectory, charge is integrated along a single line in the volume of the detector that is sampled all together by a signal collection element. The signal from each collection element is integrated over an appropriate time interval, m times per scan, so as to produce an $n \times m$ array of numbers which constitutes a two-dimensional image. Early theoretical studies and empirical studies utilizing a prototype KCD megavoltage imager with 384 6-cm-deep signal collection elements with an effective spacing of 400 μm and containing 100 atmospheres of Xe, have been reported (DiBianca *et al* 1997). These studies predict a high x-ray quantum detection efficiency ($\sim$36%) and forecast that the system would offer high spatial resolution, high contrast resolution, and negligible scatter acceptance. The authors further indicate that such systems would offer a large field of view and could be adapted to dual-energy (i.e. diagnostic and megavoltage) imaging.

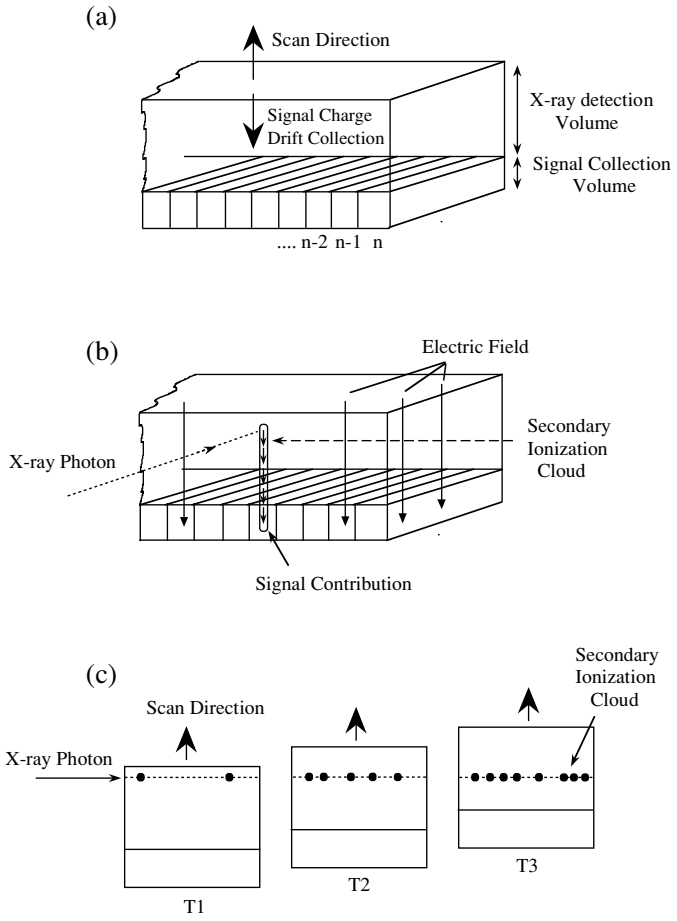

Figure 14. Schematic diagrams illustrating the kinestatic charge detection (KCD) technique. (a) Diagram of an *n*-channel KCD illustrating the x-ray detection and signal collection volumes and the anti-parallel scan and signal charge drift directions. (b) Diagram showing the drift path in the imposed electric field of a secondary ionization cloud produced by an absorbed x-ray photon. (c) Diagram of the integration over time of the charge clouds produced by interacting x-ray photons incident along a fixed trajectory. The detector moves upward as the time (labeled below) increases. Figure taken from DiBianca and Barker (1985) (reprinted with permission from AAPM).

A novel gas detector concept for portal imaging is in the early stages of development at the Karolinska Institutet (Brahme *et al* 2000, Ostling *et al* 2000, Iacobaeus *et al* 2001), with the objectives of increasing the x-ray quantum detection efficiency as well as providing dual-energy imaging. The concept incorporates the use of a gas electron multiplier (GEM)—an amplification structure recently developed by Sauli at CERN (Sauli 1997). The GEM is a simple device that provides efficient multiplication of electrons in a gas detector with a gain on the order of 10^3–10^4. One possible configuration for the imager being considered by the Karolinska group, illustrated in figure 15, consists of a single chamber filled with gas at atmospheric pressure with two parts: an upper part to image diagnostic-energy x-rays and a lower part to image megavoltage-energy x-rays. In this realization, diagnostic x-rays interact in a gas converter followed by a GEM. (In an alternate arrangement under consideration, a solid converter would be used in the upper part to provide a higher efficiency for detection

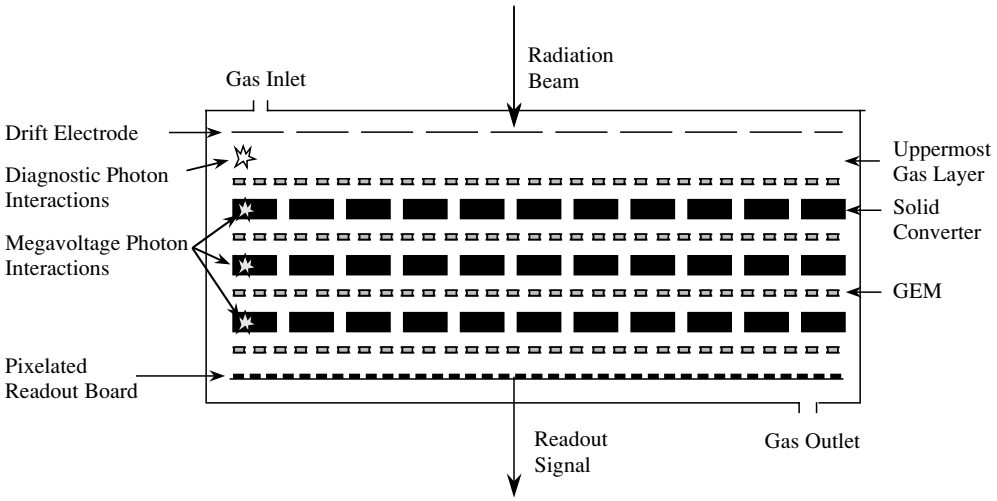

Figure 15. Schematic drawing of a possible configuration of a dual-energy device for diagnostic and portal imaging under development at the Karolinska Institutet. This configuration incorporates an upper detector for diagnostic imaging and a lower portion, consisting of three sets of solid converters and GEMs (gas electron multipliers) for portal imaging.

of diagnostic x-rays than would be achieved with gas.) In the lower part of the detector, several converter plates, followed by GEMs, are incorporated in the design to increase the detection efficiency of the megavoltage x-rays. An electric field is applied across the chamber to allow signal electrons generated by the interacting x-rays to drift down to an electronic readout plate offering 1×1 mm^2 pixelated readout. Holes in the converter plates allow signal generated above the plates to pass through to the readout plate. It is envisaged that the device will offer a 40×40 cm^2 detection area and will allow very fast readout after every radiation pulse. A possible challenge in this design would be the significantly different signal gain for x-rays interacting near the top and near the bottom of the detector leading to a form of noise associated with the conversion of x-rays.

6. Conclusion

After approximately 50 years of development, practical electronic portal imaging technologies are becoming increasingly prevalent in clinics. Interestingly, the elapsed time between initial development and widespread commercial availability of systems has, in two out of three cases, been a decade or longer. This, at least partially, reflects the considerable challenges presented by this imaging application to any candidate technology. It also reflects caution on the part of manufacturers given the relatively small size of the portal imaging market. Nevertheless, considerable motivation exists for continued development of portal imaging technology given the fact that present and imminent commercial systems have x-ray quantum detection efficiencies of less than 5% and DQEs of, at best, $\sim$1%. We anticipate that the coming years will witness the development of EPID systems offering considerably higher efficiency. Finally, it is possible that some of these future systems will represent innovative extrapolations of existing indirect and direct detection active matrix flat-panel imager technology involving considerably thicker and/or higher atomic number scintillators (such as structured scintillators incorporating CsI(Tl) in columnar or other forms) and photoconductors (such as PbI_2, HgI_2, or other candidate materials).

Acknowledgments

I wish to acknowledge the many individuals whose kind assistance made this review paper possible. Thanks to Peter Munro at the University of Western Ontario and Marcel Van Herk at the NKI for photos of and information on the commercial camera-based and matrix ionization chamber systems. Thanks also to Christian Iacobaeus and Janina Ostling for discussions concerning the GEM-based system and for providing figure 15. I also wish to thank Ed Shapiro of Varian Medical Systems, Kevin Brown of Elekta Oncology Systems, Don Carlson of Siemens Medical Systems, and Reuven Levinson of Eliav for information concerning, and pictures of their companies' systems. Finally, I wish to express special thanks to members of the flat-panel imaging group at the University of Michigan: to Youcef El-Mohri for his extensive help with the preparation of the illustrations; to Amit Sawant for valuable discusssions concerning the systems under development at the University of Tennessee and for providing figure 13; and to Youcef El-Mohri, Amit Sawant, Kyung-Wook Jee and Qihua Zhao for their assistance with proof-reading the manuscript. All these contributions were invaluable and any errors or omissions, of which there are bound to be some, are all mine.

References

Adachi S, Hori N, Sato K, Tokuda S, Sato T, Uehara K, Izumi Y, Nagata H, Yoshimura Y and Yamada S 2000 Experimental evaluation of a-Se and CdTe flat-panel x-ray detectors for digital radiography and fluoroscopy *Proc. SPIE* **3977** 38–47

Andrews J R, Swain R W and Rubin P 1958 Continuous visual monitoring of 2 MeV roentgen therapy *Am. J. Roentgenol.* **79** 74–8

Antonuk L E, Yorkston J, Boudry J, Longo M J, Jimenez J and Street R A 1990a Development of hydrogenated amorphous silicon sensors for high energy photon radiotherapy imaging *IEEE Trans. Nucl. Sci.* **37** 165–70

Antonuk L E, Boudry J, Yorkston J, Wild C F, Longo M J and Street R A 1990b Radiation damage studies of amorphous silicon photodiode sensors for applications in radiotherapy x-ray imaging *Nucl. Instrum. Methods* A **299** 143–6

Antonuk L E, Boudry J, Kim C W, Longo M J, Morton E J, Yorkston J and Street R A 1991a Signal, noise and readout considerations in the development of amorphous silicon photodiode arrays for radiotherapy and diagnostic x-ray imaging *Proc. SPIE* **1443** 108–19

Antonuk L E, Yorkston J, Boudry J, Longo M J and Street R A 1991b Large area amorphous silicon photodiode arrays for radiotherapy and diagnostic imaging *Nucl. Instrum Methods* A **310** 460–4

Antonuk L E, Yorkston J, Kim C W, Huang W, Morton E J, Longo M J and Street R A 1991c Light response characteristics of amorphous silicon arrays for megavoltage and diagnostic imaging *Mater. Res. Soc. Symp. Proc.* **219** 531–6

Antonuk L E, Boudry J, Huang W, McShan D L, Morton E J, Yorkston J, Longo M J and Street R A 1992a Demonstration of megavoltage and diagnostic x-ray imaging with hydrogenated amorphous silicon arrays *Med. Phys.* **19** 1455–66

Antonuk L E, Yorkston J, Huang W, Boudry J, Morton E J, Longo M J and Street R A 1992b Radiation response characteristics of amorphous silicon arrays for megavoltage radiotherapy imaging *IEEE Trans. Nucl Sci.* **39** 1069–73

Antonuk L E, Yorkston J, Huang W, Boudry J, Morton E J, Longo M and Street R A 1992c Factors affecting image quality for megavoltage and diagnostic x-ray a-Si:H imaging arrays *Mater. Res. Soc. Symp. Proc.* **258** 1069–74

Antonuk L E, Boudry J, Yorkston J, Morton E J, Huang W and Street R A 1992d Development of thin-film, flat-panel arrays for diagnostic and radiotherapy imaging *Proc. SPIE* **1651** 94–105

Antonuk L E, Yorkston J, Huang W, Siewerdsen J and Street R A 1993 Considerations for high frame rate operation of two-dimensional a-Si:H imaging arrays *Mater. Res. Soc. Symp. Proc.* **297** 945–50

Antonuk L E, Boudry J, Huang W, Lam K L, Morton E J, Ten Haken R K, Yorkston J and Clinthorne N H 1994 Thin-film, flat-panel, composite imagers for projection and tomographic imaging *IEEE Trans. Med. Imaging* **13** 482–90

Antonuk L E, Boudry J M, El-Mohri Y, Huang W, Siewerdsen J H, Yorkston J and Street R A 1995 Large area, flat-panel amorphous silicon imagers *Proc. SPIE* **2432** 216–27

Antonuk L E, Yorkston J, Huang W, Sandler H, Siewerdsen J H and El-Mohri Y 1996 Megavoltage imaging with a large area, flat-panel, amorphous silicon imager *Int. J. Radiat. Oncol. Biol. Phys.* **36** 661–72

Antonuk L E, El-Mohri Y, Huang W, Jee K-W, Siewerdsen J H, Maolinbay M, Scarpine V E, Sandler H and Yorkston J 1998a Initial performance evaluation of an indirect-detection, active matrix flat-panel imager (AMFPI) prototype for megavoltage imaging *Int. J. Radiat. Oncol. Biol. Phys.* **42** 437–54

Antonuk L E, El-Mohri Y and Jee K-W 1998b Active matrix flat-panel imagers for electronic portal imaging (AMFPIs) *Imaging in Radiation Therapy* AAPM Medical Physics Monograph no 24 ed John D Hazel and Arthur L Boyer (Medical Physics Publishing) 371–92

Baily N A, Horn R A and Kampp T D 1980 Fluoroscopic visualization of megavoltage therapeutic x-ray beams *Int. J. Radiat. Oncol. Biol. Phys.* **6** 935–9

Benner S, Rosengren B, Wallman H and Netteland O 1962 Television monitoring of a 30 MV x-ray beam *Phys. Med. Biol.* **7** 29–34

Bissonnette J-P, Jaffray D A, Fenster A and Munro P 1994 Optimal radiographic magnification for portal imaging *Med. Phys.* **21** 1435–45

Bissonnette J-P, Cunningham I A and Munro P 1997a Optimal phosphor thickness for portal imaging *Med. Phys.* **24** 803–14

Bissonnette J-P, Cunningham I A, Jaffray D A, Fenster A and Munro P 1997b A quantum accounting and detective quantum efficiency analysis for video-based portal imaging *Med. Phys.* **24** 815–86

Boudry J M and Antonuk L E 1994 Radiation damage of amorphous silicon photodiode sensors *IEEE Trans. Nucl. Sci.* **41** 703–7

Boudry J M and Antonuk L E 1996 Radiation damage of amorphous silicon, thin-film, field-effect transistors *Med. Phys.* **23** 743–54

Boyer A L, Antonuk L, Fenster A, Meertens H, Munro P, Reinstein L E and Wong J 1992 A review of electronic portal imaging devices (EPIDs) *Med. Phys.* **19** 1–16

Brahme A, Danielsson M, Iacobaeus C, Ostling J, Peskov V and Wallmark M 2000 Evaluation of a GEM and CAT-based detector for radiation therapy beam monitoring *Nucl. Instrum. Methods* A **454** 136–41

Choquette M, Rougeot H, Martin J P, Laperriere L, Shukri Z and Polischuk B 2000 Direct selenium x-ray detector for fluoroscopy, R&F, and radiography *Proc. SPIE* **3977** 128–36

Colbeth R E, Allen M J, Day D J, Gilblom D L, Klausmeier-Brown M E, Pavkovich J, Seppi E J and Shapiro E G 1997 Characterization of an amorphous silicon fluoroscopic imager *Proc. SPIE* **3032** 42–51

Cunningham I A, Westmore M S and Fenster A 1994 A spatial-frequency dependent quantum accounting diagram and detective quantum efficiency model of signal and noise propagation in cascaded imaging systems *Med. Phys.* **21** 417–27

Cunningham I A and Shaw R 1999 Signal-to-noise optimization of medical imaging systems *J. Opt. Soc. Am.* A **16** 621–32

DiBianca F A and Barker M D 1985 Kinestatic charge detection *Med. Phys.* **12** 339–43

DiBianca F *et al* 1996 Initial clinical performance of a large-field KCD digital radiography system *Proc. SPIE* **2708** 826–36

DiBianca F, Samant S, Laughter J, Rasmussen J and Rodriguez C 1997 Use of a kinestatic charge detector for megavoltage portal imaging *Proc. SPIE* **3032** 195–201

Dickerson R E, Haus A G and Huff K E 1997 Development of a novel, high contrast, cassette/film/screen system for radiation therapy portal localization imaging *Proc. SPIE* **3032** 520–9

Dobbins J T, Ergun D L, Rutz L, Hinshaw D A, Blume H and Clark D C 1995 DQE(f) of four generations of computed radiography acquisition devices *Med. Phys.* **22** 1581–93

Drake D G, Jaffray D A and Wong J 1997 A prototype amorphous silicon array based radiotherapy portal imager *Proc. SPIE* **3032** 32–41

Drake D G, Jaffray D A and Wong J W 2000 Characterization of a fluoroscopic imaging system for kV and MV radiography *Med. Phys.* **27** 898–05

Earnhart J R D and Chaney E L 1997 Modulation transfer function for a large-area amorphous silicon image receptor *Phys. Med. Biol.* **42** 2531–40

El-Mohri Y, Antonuk L E, Yorkston J, Jee K W, Maolinbay M, Lam K L and Siewerdsen J H 1999 Relative dosimetry using active matrix flat-panel imager (AMFPI) technology *Med. Phys.* **26** 1530–41

El-Mohri Y, Jee K-W, Antonuk L E, Maolinbay M and Zhao 2001 Determination of the detective quantum efficiency of a prototype megavoltage indirect detection, active matrix flat-panel imager *Med. Phys.* **28** 2538–50

Entine G, Redus R H, Feyder A and Biggs P J 1993 Recent results with a CdTe imaging portal scanner for radiation therapy *IEEE Trans. Nucl. Sci.* **40** 1012–6

Entine G, Squillante M R, Hahn R, Cirignano L J, McGann W and Biggs P J 1992 High contrast, CdTe portal scanner for radiation therapy *IEEE Trans. Nucl. Sci.* **39** 1480–4

Evans P M, Donovan E M, Partridge M, Childs P J, Convery D J, Eagle S, Hansen V N, Suter B L and Yarnold J R 2000 The delivery of intensity modulated radiotherapy to the breast using multiple static fields *Radiother. Oncol.* **57** 79–89

Evans P M, Gildersleve J Q, Morton E J, Swindell W, Coles R, Ferraro M, Rawlings C, Xiao Z R and Dyer J 1992 Image comparison techniques for use with megavoltage imaging systems *Br. J. Radiol.* **65** 701–9

Ezz A, Munro P, Porter A T, Battista J, Jaffray D A, Fenster A and Osborne S 1991 Daily monitoring and correction of radiation field placement using a video-based portal imaging system: a pilot study *Int. J. Radiat. Oncol. Biol. Phys.* **22** 159–65

Falco T, Wang H and Fallone B G 1998 Preliminary study of a metal/a-Se-based portal detector *Med. Phys.* **25** 814–23

Hansen V N, Evans P M and Swindell W 1996 The application of transit dosimetry to precision radiotherapy *Med. Phys.* **23** 713–21

Heijmen B J M, Pasma K L, Kroonwijk M, Althof V G, de Boer J C, Visser A G and Huizenga H 1995 Portal dose measurement in radiotherapy using an electronic portal imaging device (EPID) *Phys. Med. Biol.* **40** 1943–55

Heijmen B J M, Visser A G and Huizenga H 1992 *In vivo* dose measurements using an electronic portal imaging device: A feasibility study (Abstract) *Radiother. Oncol.* **24** (suppl) S25

Herman M G, Balter J M, Jaffray D A, McGee K P, Munro P, Shalev S, Van Herk M and Wong J W 2001 Clinical use of electronic portal imaging: report of AAPM radiation therapy committee task group 58 *Med. Phys.* **28** 712–37

Iacobaeus C, Brahme A, Danielsson M, Fonte P, Ostling J, Peskov V and Wallmark M 2001 A novel portal imaging device for advanced radiation therapy *IEEE Trans. Nucl. Sci.* **48** 1496–502

Jaffray D A, Battista J J, Fenster A and Munro P 1995a Monte Carlo studies of x-ray energy absorption and quantum noise in megavoltage transmission radiography *Med. Phys.* **22** 1077–89

Jaffray D A, Chawla K, Yu C and Wong J W 1995b Dual-beam imaging for online verification of radiotherapy field placement *Int. J. Radiat. Oncol. Biol. Phys.* **33** 1273–80

Lachaine M and Fallone B G 1998 Monte Carlo detective quantum efficiency and scatter studies of a metal/a-Se portal detector *Med. Phys.* **25** 1186–94

Lachaine M, Fourkal E and Fallone B G 2001 Investigation into the physical characteristics of active matrix flat panel imagers for radiotherapy *Med. Phys.* **28** 1689–95

Lam K S, Partowmah M and Lam W C 1986 An on-line electronic portal imaging system for external beam radiotherapy *Br. J. Radiol.* **59** 1007–13

Lam W C, Partowmah M, Lee D J, Wharam M D and Lam K S 1987 On-line measurement of field placement errors in external beam radiotherapy *Br. J. Radiol.* **60** 361–5

Leong J 1986 Use of digital fluoroscopy as an on-line verification device in radiation therapy *Phys. Med. Biol.* **31** 985–92

Lewis D G, Swindell W, Morton E J, Evans P M and Xiao Z R 1992 A megavoltage CT scanner for radiotherapy verification *Phys. Med. Biol.* **37** 1985–99

Mah D, Rowlands J A and Rawlinson J A 1998 Sensitivity of amorphous selenium to x rays from 40 kVp to 18 MV: measurements and implications for portal imaging *Med. Phys.* **25** 444–56

Mah D, Rawlinson J A and Rowlands J A 1999 Detective quantum efficiency of an amorphous selenium detector to megavoltage radiation *Phys. Med. Biol.* **44** 1369–84

McCurdy B M C, Luchka K and Pistorius S 2001 Dosimetric investigation and portal dose image prediction using an amorphous silicon electronic portal imaging device *Med. Phys.* **28** 911–24

Meertens H, van Herk M and Weeda J 1985 A liquid ionization detector for digital radiography of therapeutic megavoltage photon beams *Phys. Med. Biol.* **30** 313–21

Meertens H, van Herk M, Bijhold J and Bartelink H 1990 First clinical experience with a newly developed electronic portal imaging technology *Int. J. Radiat. Oncol. Biol. Phys.* **18** 1173–81

Metz C E, Wagner R F, Doi D, Brown D G, Nishikawa R M and Myers K J 1995 Towards consensus on quantitative assessment of medical imaging systems *Med. Phys.* **22** 1057–61

Morton E J and Swindell W 1987 A digital system for the production of radiotherapy verification images *Proc. 9th Int. Conf. on the Use of Computers in Radiation Therapy* vol 375 (Amsterdam: Elsevier) pp 375–7

Morton E J 1988 A digital system for the production of radiotherapy verification images *PhD Thesis* University of London

Morton E J, Swindell W, Lewis D G and Evans P M 1991 A linear scintillation-crystal photodiode detector for radiotherapy imaging *Med. Phys.* **18** 681–91

Mosleh-Shirazi M A, Swindell W and Evans P M 1994 Monte Carlo simulations of CsI(Tl) scintillation crystals for use in a three-dimensional megavoltage CT scanner *Nucl. Instrum. Methods* A **348** 563–6

Mosleh-Shirazi M A, Swindell W and Evans P M 1998a Optimization of the scintillation detector in a combined 3D megavoltage CT scanner and portal imager *Med. Phys.* **25** 1880–90

Mosleh-Shirazi M A, Evans P M, Swindell W, Symonds-Tayler J R N, Webb S and Partridge M 1998b Rapid portal imaging with a high-efficiency, large field of view detector *Med. Phys.* **25** 2333–46

Mulato M, Ready S, Van Schuylenbergh K, Lu J P and Street R A 2001 Cross-talk and lateral conduction effects in continuous-sensor amorphous silicon imagers *J. Appl. Phys.* **89** 8193–201

Munro P, Rawlinson J A and Fenster A 1987 Therapy imaging: a signal-to-noise analysis of metal plate/film detectors *Med. Phys.* **14** 975–84

Munro P, Rawlinson J A and Fenster A 1988 Therapy imaging: source sizes of radiotherapy beams *Med. Phys.* **15** 517–24

Munro P, Rawlinson J A and Fenster A 1990a Therapy imaging: a signal-to-noise analysis of a fluoroscopic imaging system for radiotherapy localization *Med. Phys.* **17** 673–772

Munro P, Rawlinson J A and Fenster A 1990b A digital fluoroscopic imaging device for radiotherapy localization *Int. J. Radiat. Oncol. Biol. Phys.* **18** 641–9

Munro P 1995 Portal imaging technology: past, present, and future *Semin. Radiat. Oncol.* **5** 115–33

Munro P and Bouius D C 1998a X-ray quantum limited portal imaging using amorphous silicon flat panel arrays *Med. Phys.* **25** 689–702

Munro P, Bouius D C, Moseley J, Martin L, Zhang Y and Jaffray D A 1998b Glaring errors in transit dosimetry (Abstract) *Med. Phys.* **25** 1097

Munro P 1999 Megavoltage radiography for treatment verification *The Modern Technology of Radiation Oncology—A Compendium for Medical Physicists and Radiation Oncologists* ed J Van Dyk (Madison: Medical Physics Publishing) ch 13

Ostling J, Wallmark M, Brahme A, Danielsson M, Iacobaeus C, Fonte P and Peskov V 2000 Novel detector for portal imaging in radiation therapy *Proc. SPIE* **3977** 84–95

Pang G, Lee D L and Rowlands J A 2001 Investigation of a direct conversion flat panel imager for portal imaging *Med. Phys.* **28** 2121–8

Pang G and Rowlands J A 2000 Electronic portal imaging with an avalanche-multiplication-based video camera *Med. Phys.* **27** 676–84

Radcliffe T, Barnea G, Wowk B, Rajapakshe R and Shalev S 1993 Monte Carlo optimization of metal/phosphor screens at megavoltage energies *Med. Phys.* **20** 1161–9

Roehrig H and Cheng C-W 1993 Real-time imaging detectors for portal imaging *Proc. SPIE* **2009** 144–67

Rogers D W O 1984 Fluence to dose equivalent conversion factors calculated with EGS3 for electrons from 100 keV to 20 GeV and photons from 11 keV to 20 Gev *Health Phys.* **46** 891–914

Samant S S, Zheng W, DiBianca F A, Zeman H D and Laughter J L 1999 A new calibration technique for KCD-based megavoltage imaging *Proc. SPIE* **3659** 779–92

Sauli F 1997 GEM: a new concept for electron amplification in gas detectors *Nucl. Instrum. Methods* A **386** 531–4

Sawant A 1999 Portal Imaging using a CsI(Tl) scintillator coupled to a cooled CCD camera *Masters Thesis* University of Tennessee, Memphis

Sawant A, Zeman H, Samant S, Lovhoiden G, Weinberg B and DiBianca F 2002 Theoretical analysis and experimental evaluation of a CsI(Tl) based electronic portal imaging system *Med. Phys.* at press

Shalev S, Lee T, Leszczynski K, Cosby S, Chu T, Reinstein L and Meek A 1989 Video techniques for on-line portal imaging *Comput. Med. Imaging Graph* **13** 217–6

Shalev S 1995 Treatment verification using digital imaging *Medical Radiology Radiation Therapy Physics* ed A R Smith (Berlin: Springer) ch 8

Shaw R and Dainty J C 1976 *Image Science* (San Diego: Academic) pp 152–89

Siewerdsen J H 1998 Signal, noise, and detective quantum efficiency of a-Si:H flat-panel imagers *Thesis* University of Michigan

Spies L, Evans P M, Partridge M, Hansen V N and Bortfeld T 2000 Direct measurement and analytical modeling of scatter in portal imaging *Med. Phys.* **27** 462–71

Strandqvist M and Rosengren B 1958 Television-controlled pendulum therapy *Br. J. Radiol.* **31** 513–4

Street R A, Nelson S, Antonuk L E and Perez Mendez V 1990 Amorphous silicon sensor arrays for radiation imaging *Mater. Res. Soc. Symp. Proc.* **192** 441–52

Street R A 1991 *Hydrogenated Amorphous Silicon* (Cambridge: Cambridge University Press)

Street R A (ed) 2000 *Technology and Applications of Amorphous Silicon (Springer Series in Materials Science)* vol 37 (Berlin: Springer)

Street R A, Mulato M, Schieber M, Hermon H, Shah K, Bennett P, Dmitryev Y, Ho J, Lau R, Meerson E, Ready S E, Reisman B, Sado Y, VanSchuylenbergh K, Vilensky A and Zuck A 2001 Comparative study of PbI_2 and HgI_2 as direct detector materials for high resolution x-ray image sensors *Proc. SPIE* **4320** 1–12

Swindell W 1991 The lens coupling efficiency in megavoltage imaging *Med. Phys.* **18** 1152–3

Swindell W, Morton E J, Evans P M and Lewis D G 1991 The design of megavoltage projection imaging systems: some theoretical aspects *Med. Phys.* **18** 855–66

Symonds-Tayler J R N, Partridge M and Evans P M 1997 An electronic portal imaging device for transit dosimetry *Phys. Med. Biol.* **42** 2273–83

Taborsky S C, Lam W C, Sterner R E and Skarda G M 1982 Digital imaging for radiation therapy verification *Opt. Eng.* **21** 888–93

Tsukamoto A, Yamada S, Tomisaki T, Tanaka M, Sakaguchi T, Asahina H, Suzuki K and Ikeda M 1999 Development and evaluation of a large-area selenium-based flat-panel detector for real-time radiography and fluoroscopy *Proc. SPIE* **3659** 14–23

Van Herk M and Meertens 1987 A digital imaging system for portal verification *Proc. 9th Int. Conf. on the Use of Computers in Radiation Therapy* (Amsterdam: Elsevier) pp 371–4

Van Herk M and Meertens M 1988 A matrix ionisation chamber imaging device for on-line patient setup verification during radiotherapy *Radiother. Oncol.* **11** 369–78

Van Herk M 1991 Physical aspects of a liquid-filled ionization chamber with pulsed polarizing voltage *Med. Phys.* **18** 692–702

Van Herk M, Bijhold J, Hoogervorst B and Meertens H 1992 Sampling methods for a matrix ionization chamber system *Med. Phys.* **19** 409–18

Van Herk M 2001 Private communication

Wallman H and Stalberg N 1958 A television-roentgen system for pendulum therapy *Br. J. Radiol.* **31** 576–7

Webb S 1993 Megavoltage portal imaging *The Physics Of Three-Dimensional Radiation Therapy* (Bristol: Institute of Physics Publishing)

Wong J W, Binns W R, Cheng A Y, Gear L Y, Epstein J W, Klarmann J and Purdy J A 1990 On-line radiotherapy imaging with an array of fibre-optic image reducers *Int. J. Radiat. Oncol. Biol. Phys.* **18** 1477–84

Wong J W, Cheng A Y, Binns W R, Epstein J W, Klarmann J and Perez C A 1993 Development of a second-generation fiber-optic on-line verification system *Int. J. Radiat. Oncol. Biol. Phys.* **26** 311–20

Wowk B, Shalev S and Radcliffe T 1993 Grooved phosphor screens for on-line portal imaging *Med. Phys.* **20** 1641–51

Wowk B, Radcliffe T, Leszczynski K W, Shalev S and Rajapakshe R 1994 Optimization of metal/phosphor screens for on-line portal imaging *Med. Phys.* **21** 227–35

Zeman H D, Samant S S, Lovhoiden G, Weinberg B and Sawant A 1998 Portal Imaging with a CsI(Tl) transparent scintillator x-ray detector *Proc. SPIE* **3336** 175–86

Zhao W and Rowlands J A 1995 X-ray imaging using amorphous selenium: feasibility of a flat-panel self-scanned detector for digital radiology *Med. Phys.* **22** 1595–1604